Article

Cell Reports

Distinct Roles for *Rac1* in Sertoli Cell Function during Testicular Development and Spermatogenesis

Graphical Abstract

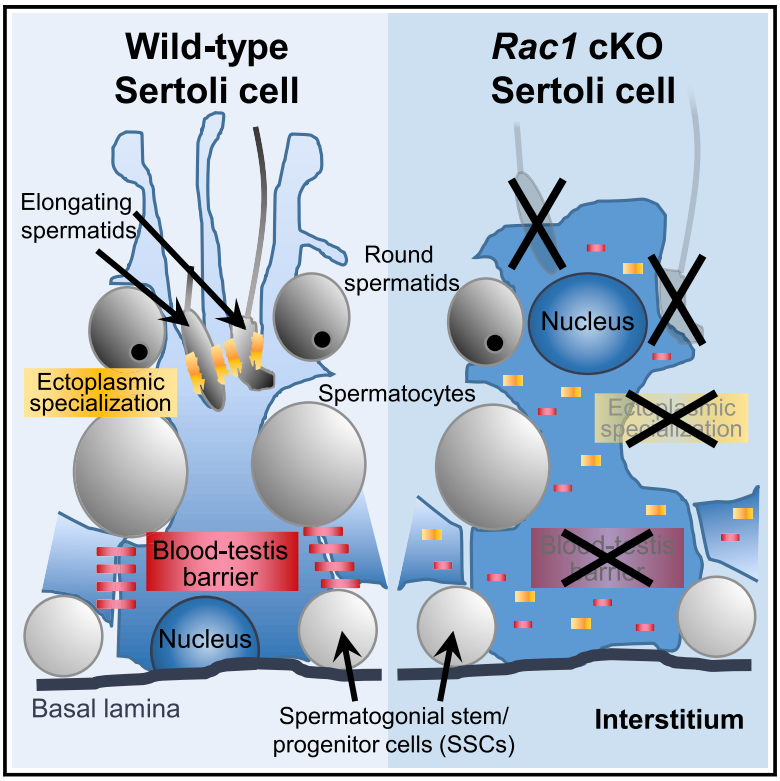

Authors

Anna Heinrich, Sarah J. Potter, Li Guo, Nancy Ratner, Tony DeFalco

Correspondence

tony.defalco@cchmc.org

In Brief

Testicular Sertoli cells are polarized supporting cells that simultaneously support germ cells at various stages of differentiation. Heinrich et al. use a Sertoli-specific conditional deletion of *Rac1*, a Rho GTPase required for apicobasal cell polarity, to reveal the distinct requirements for Sertoli cell polarity during testicular differentiation and function.

Highlights

- Sertoli *Rac1* function is required for later stages of spermatogenesis
- *Rac1*-deficient Sertoli cells exhibit severe defects in apicobasal cell polarity
- *Rac1* is dispensable for testis differentiation and germline stem cell maintenance
- Fetal Sertoli cells do not yet show hallmarks of complete apicobasal cell polarity

Heinrich et al., 2020, Cell Reports *31*, 107513
April 14, 2020
https://doi.org/10.1016/j.celrep.2020.03.077

CellPress

Cell Reports
Article

Distinct Roles for *Rac1* in Sertoli Cell Function during Testicular Development and Spermatogenesis

Anna Heinrich,[1] Sarah J. Potter,[1] Li Guo,[2] Nancy Ratner,[2,3] and Tony DeFalco[1,3,4,*]
[1]Division of Reproductive Sciences, Cincinnati Children's Hospital Medical Center, Cincinnati, OH 45229, USA
[2]Division of Experimental Hematology and Cancer Biology, Cincinnati Children's Hospital Medical Center, Cincinnati, OH 45229, USA
[3]Department of Pediatrics, University of Cincinnati College of Medicine, Cincinnati, OH 45267, USA
[4]Lead Contact
*Correspondence: tony.defalco@cchmc.org
https://doi.org/10.1016/j.celrep.2020.03.077

SUMMARY

Sertoli cells are supporting cells of the testicular seminiferous tubules, which provide a nurturing environment for spermatogenesis. Adult Sertoli cells are polarized so that they can simultaneously support earlier-stage spermatogenic cells (e.g., spermatogonia) basally and later-stage cells (e.g., spermatids) apically. To test the consequences of disrupting cell polarity in Sertoli cells, we perform a Sertoli-specific conditional deletion of *Rac1*, which encodes a Rho GTPase required for apicobasal cell polarity. *Rac1* conditional knockout adults exhibit spermatogenic arrest at the round spermatid stage, with severe disruption of Sertoli cell polarity, and show increased germline and Sertoli cell apoptosis. Thus, Sertoli *Rac1* function is critical for the progression of spermatogenesis but, surprisingly, is dispensable for fetal testicular development, adult maintenance of undifferentiated spermatogonia, and meiotic entry. Our data indicate that Sertoli *Rac1* function is required only for certain aspects of spermatogenesis and reveal that there are distinct requirements for cell polarity during cellular differentiation.

INTRODUCTION

Sertoli cells are supporting cells that intimately communicate with the male germline and nurture its development from prospermatogonia into sperm. Sertoli cells are the first sex-specific cell type detected in the fetal testis and express sex determination genes such as *Sry* and *Sox9*, which drive bipotential gonadal somatic cells toward the Sertoli pathway (Albrecht and Eicher, 2001). Sertoli cells and germ cells *in utero* form testis cords, which are tubule-like structures that hollow out at approximately postnatal day 14 (P14) to form the seminiferous tubules, the sites of spermatogenesis that represent the functional units of the mammalian testis (Cool et al., 2012).

At different stages of life, Sertoli cells have unique properties that enable them to perform various functions. During fetal stages into the first 2 weeks of postnatal life in mice, Sertoli cells actively divide and increase in number (Kluin et al., 1984; Orth, 1982), so that they can establish niches for spermatogonial stem and progenitor cells. By 2 weeks of age, Sertoli cells enter into mitotic arrest and exit the cell cycle, and do not re-enter active cell cycle in adulthood. Upon maturation under the influence of hormones such as testosterone, insulin-like growth factor 1 (IGF1), follicle-stimulating hormone (FSH), and others, Sertoli cells undergo a number of changes, including downregulation of the SOX9 target gene *Amh*, upregulation of the transcription factor GATA1, and nuclear translocation of the androgen receptor (AR) (Sharpe et al., 2003). In addition, Sertoli cells form the blood-testis barrier (BTB), which is a series of tight junctions that physically sequester meiotic and post-meiotic germ cells within the luminal compartment of the tubule. Given that neo-antigens from meiotic and post-meiotic cells likely arise after the establishment of tolerance, a functional BTB is required to prevent deleterious immune infiltrate into the seminiferous tubules. The BTB is also called the basal ectoplasmic specialization (ES), which is a unique Sertoli-Sertoli structure, separate from the apical ES, which is a Sertoli cell-germ cell F-actin cytoskeletal structure that ensures the proper attachment and alignment of developing spermatids to the Sertoli cell before spermiation (Gao and Cheng, 2016; Russell et al., 1988).

Spermatogenesis is a series of proliferative and differentiating steps that lead to the formation of spermatozoa from a germline stem cell population called spermatogonial stem cells (SSCs) or, more broadly, as a stem-progenitor population called undifferentiated spermatogonia (Kanatsu-Shinohara and Shinohara, 2013). Under the influence of glial-derived neurotrophic factor (GDNF) secreted from Sertoli and peritubular myoid cells (Chen et al., 2014, 2016; Meng et al., 2000), SSCs are maintained in the basal-most compartment of the seminiferous tubule, where they transition into transit-amplifying undifferentiated spermatogonia, and then, under the influence of retinoic acid (RA), into differentiating spermatogonia. Later, also in response to RA, they subsequently progress into preleptotene spermatocytes, at which point they transit across the BTB into the adluminal compartment of the tubule. The adluminal compartment contains all of the spermatocyte populations, in addition to round, elongating, and condensing spermatids just before spermiation and release from Sertoli cells as testicular spermatozoa (reviewed in França et al., 2016; Oatley and Brinster, 2012).

Each Sertoli cell can support a species-specific, limited number of germ cells, ranging from 11 in humans to 35 in mice (reviewed in França et al., 2016). The maximum capacity of spermatogenesis and the number of SSC niches within the testis is largely dictated by the number of Sertoli cells, as has been

demonstrated in rodent models of hypothyroidism that increase Sertoli cell number (Hess et al., 1993; Joyce et al., 1993; Oatley et al., 2011). Each Sertoli cell simultaneously interacts with undifferentiated spermatogonia, differentiating spermatogonia, meiotic spermatocytes, and post-meiotic spermatids in the mammalian testis, which requires extensive apicobasal polarity. Sertoli cell polarity is evident by the specific localization of tight-junction components in the BTB, as well as the specific apical or basal compartmental localization of at least 3 separate polarity protein complexes: the PAR3/PAR6/aPKC complex, the Crumbs/PATJ/PALS1 complex, and the Scribble (SCRIB)/DLG/LGL complex (Gao et al., 2016a; Su et al., 2012; Wong et al., 2008). Activity of the PAR3 and Crumbs complexes promotes BTB function, while activity of the SCRIB complex is upregulated upon disassembly of the BTB during stages VII–VIII, when germ cells transit through the BTB upon entry into meiosis (Gao et al., 2016b). Therefore, the localization and function of these three polarity complexes are critical for Sertoli cell apicobasal polarity and the progression of spermatogenesis (Gao et al., 2016a; Su et al., 2012; Wong et al., 2008).

Another family of proteins that is linked to cell polarity are the Rho GTPases, which have a functionally diverse repertoire of potential cellular functions, including regulation of the actin cytoskeleton, cell movement, cell adhesion, cell division, cell death or survival, and membrane trafficking (Ngok et al., 2014). One of the most well-known members of this family is RAC1. *Rac1* has a broad range of roles in development and disease, but little is known about the specific function of *Rac1* in reproduction. *Rac1* is required in SSCs to transmigrate the BTB during testicular germline transplantation, but is also expressed in adult Sertoli cells (Takashima et al., 2011). Recently, a study of a Sertoli cell-specific conditional deletion of *Raptor*, an essential component of the mechanistic target of rapamycin kinase complex 1 (mTORC1) pathway, proposed that RAC1 acts downstream of mTORC1 to establish Sertoli cell cytoarchitecture (Xiong et al., 2018). However, specific roles for *Rac1* in spermatogenesis are not well defined; additionally, the idea that cell polarity is required for spermatogenesis is generally well appreciated, but the timing of its action developmentally is not well understood.

In this study, we show that *Rac1* function in Sertoli cells has specific and distinct roles in spermatogenesis. *Rac1*-deficient Sertoli cells can proliferate in the fetal testis and are present in the fetal and postnatal testis, but in adults show severe defects in cell polarity, as manifested by mislocalization of polarity protein complexes and disruption of the BTB. Sertoli *Rac1* function is, surprisingly, not required for the maintenance of undifferentiated spermatogonia in the adult testis nor for germ cell entry into meiosis. In addition, *Rac1* function in Sertoli cells is dispensable for fetal testicular differentiation, suggesting that Sertoli *Rac1* is not absolutely required for early somatic and germline differentiation in the testis or for early stages of steady-state spermatogenesis. *Rac1* is, in contrast, required for the progression of spermatogenesis past the round spermatid stage, likely due to polarity defects in Sertoli cells. Overall, these findings suggest that *Rac1* has differential functions in Sertoli cells and also indicate that Sertoli cell polarity is dispensable for certain aspects of spermatogenesis and testicular function.

RESULTS

Dhh-Cre Is Highly Specific and Efficient at Targeting Sertoli Cells Starting at the Onset of Testicular Differentiation

We and others have shown, through cell-type-specific transcriptomic analyses (Jameson et al., 2012) (Figure S1A) and single-cell RNA sequencing (Stévant et al., 2018) of fetal testicular cells, that *Rac1* is expressed in Sertoli cells throughout all stages analyzed (embryonic day [E]11.5–E16.5); additionally, a study demonstrated that RAC1 is expressed in adult Sertoli cells (Takashima et al., 2011). Therefore, *Rac1* may function in Sertoli cells at any point between fetal testis differentiation and adulthood. To target *Rac1* specifically within Sertoli cells, we used a Cre line driven by *Dhh* (*Dhh*-Cre), which is active in Sertoli cells starting early in testicular differentiation (Figure S1B). Using a Cre-responsive *Rosa*-tdTomato reporter mouse line, we confirmed that *Dhh*-Cre is active starting by at least E12.5, immediately after testis differentiation has begun, specifically in $SOX9^+$ Sertoli cells (Figure S1C). In addition, we lineage traced *Dhh*-Cre-expressing cells into adulthood (3 months of age) and determined that Cre activity is almost 100% efficient in Sertoli cells, with no activity observed in germ cells or interstitial cells (Figures S1D–S1I).

Rac1 Function Is Required for Sertoli Cell Development in the Adult Testis

In 3-month-old adult *Dhh*-Cre;$Rac1^{flox/flox}$ conditional knockout (cKO) males, we observed that testicular development was severely disrupted: cKO testis weight was significantly reduced (~85% reduction) relative to control littermates, the tubule cross-sectional area was reduced by 75%, and there were approximately 25% fewer $SOX9^+$ Sertoli cells per tubule (Figures 1A, 1B, and 1K–1M). Consistent with decreased tubule contribution to the testis, we observed a greater proportion of interstitial tissue, which contained Leydig cells, peritubular myoid cells, and vasculature, in testicular cross-sections of cKO testes as compared to controls at various postnatal and adult stages (Figures S2A–S2F, and S2H–S2O). In particular, quantification revealed a significant increase in the number of Leydig cells relative to seminiferous tubules in cKO testes (Figure S2R).

To determine whether there were any defects in Sertoli cell differentiation in *Rac1* cKO testes, we examined the expression of several Sertoli-specific markers. We found that the Sertoli cell maturation marker GATA1 was expressed in cKO Sertoli cells, although GATA1 was expressed in all of the tubules within the cKO testis, as opposed to expression in a subset of tubules in control testes (Figures 1C and 1D), which is regulated by feedback from differentiated germ cells in various stages of spermatogenesis (Yomogida et al., 1994). While anti-Müllerian hormone (AMH), which is normally downregulated in the mature testis, was not ectopically expressed (Figures 1E and 1F), we observed strong expression of GDNF, which is required for the maintenance of SSCs (Figures 1G and 1H). Quantitative real-time PCR did not indicate any increase in *Gdnf* mRNA levels relative to control testes (Figure S3), suggesting that strong GDNF staining was likely because of denser Sertoli cell cytoplasm in cKO tubules due to a reduced number of germ cells

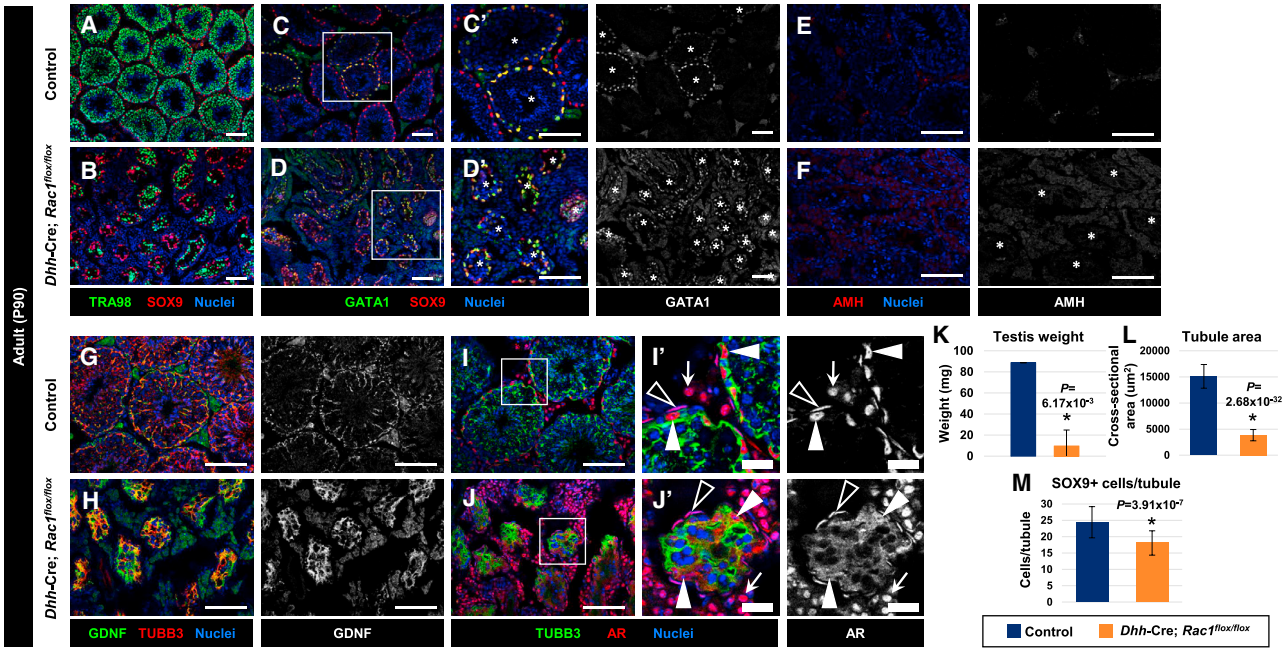

Figure 1. Sertoli *Rac1* Function Is Required for Proper Adult Testicular Development

(A–J) Three-month-old (P90) control *Dhh*-Cre;*Rac1*$^{flox/+}$ (A, C, E, G, and I) and *Dhh*-Cre;*Rac1*$^{flox/flox}$ (cKO) (B, D, F, H, and J) testes. (C'), (D'), (I'), and (J') are higher-magnification images of the boxed regions in (C), (D), (I), and (J).

(A and B) Relative to controls (A), *Rac1* cKO testes (B) exhibit smaller tubules with varying numbers of TRA98^{+} germ cells.

(C and D) *Rac1* cKO testes (D) show GATA1 expression in all tubules, in contrast to heterogeneous expression in controls (C). Asterisks indicate tubules containing GATA1^{+} Sertoli cells.

(E and F) *Rac1* cKO testes (F) express AMH at similar levels to controls (E). Asterisks indicate tubules in (F).

(G and H) *Rac1* cKO tubules (H) show robust expression of GDNF within Sertoli cells, similar to controls (G).

(I and J) Relative to controls (I), cKO testes (J) show abnormal cytoplasmic localization of AR in Sertoli cells (white arrowheads), but normal nuclear localization of AR in peritubular myoid cells (black arrowheads) and Leydig cells (white arrows). Thin scale bar, 100 μm; thick scale bar, 25 μm.

(K) Average testis weight of P90 control (*Rac1*$^{flox/flox}$) males versus cKO males (n = 3 testes for controls and n = 2 testes for cKO, each from independent males).

(L and M) (L) Average tubule cross-sectional area of P90 control (*Dhh*-Cre;*Rac1*$^{flox/+}$) versus cKO tubules (n = 10 tubules each from 3 independent males). (M) Cell counts of SOX9^{+} cells per tubule in P90 control (*Dhh*-Cre;*Rac1*$^{flox/+}$) versus cKO testes (n = 10 tubules each from 3 independent males).

The data in (K)–(M) are shown as means ± SDs. p values were performed via a two-tailed Student's t test.

See also Figures S1–S3.

(Figures 1A and 1B). In addition, we saw that AR, which is nuclear localized within Sertoli cells in control testes, was localized diffusely throughout the entire Sertoli cell within cKO testes (Figures 1I and 1J), indicating some defects in Sertoli cell development or function. Initial quantitative real-time PCR analyses suggested that *Sox9* and *Ar* expression were upregulated (Figure S3A), which was probably due to an increase in the relative proportion of Sertoli cells relative to other cells in cKO testes after a loss in germ cells; however, when normalized to *Sox9* expression to account for changes in Sertoli cell contribution to the total testis due to the loss of germ cells, there was no significant *Ar* upregulation (Figure S3B).

Rac1 Is Not Required for the Onset of Quiescence in Postnatal Sertoli Cells

As *Rac1* has been proposed to promote cell-cycle progression and cell division (Michaelson et al., 2008; Olson et al., 1995), we examined whether Sertoli cells in *Rac1* cKO adults showed altered cell-cycle status. In 3-month-old cKO testes, we saw that Sertoli cells were consistently MKI67^{-}, similar to control littermate testes (Figures 2A and 2B). We also observed that germ cells remained in active cell cycle in cKO testes, similar to controls (Figures 2C and 2D). Since Sertoli cells normally enter cell-cycle quiescence at around 2 weeks of age, we also assessed whether there was a change in the timing of quiescence in postnatal cKO males. cKO testes at both P18 and P24 appeared similar to controls, in which all Sertoli cells were MI67^{-} (Figures 2E–2H), suggesting that the onset of quiescence occurred at the proper timing in cKO Sertoli cells.

Rac1 Conditional Deletion Leads to Increased Cell Death in the Testis

To assess whether there was increased apoptosis in cKO testes, we examined the levels of cleaved caspase 3. While there were few apoptotic cells in control testes, there was increased cell death in the testes of cKO mice (Figures 2I–2M). Co-stains with Sertoli and germ cell markers suggested that increased cell death in cKO testes was occurring slightly more often in Sertoli cells, as compared to germ cells (Figures 2I–2M). While apoptotic germ (TRA98^{+}) cells occurred regularly in cKO testes,

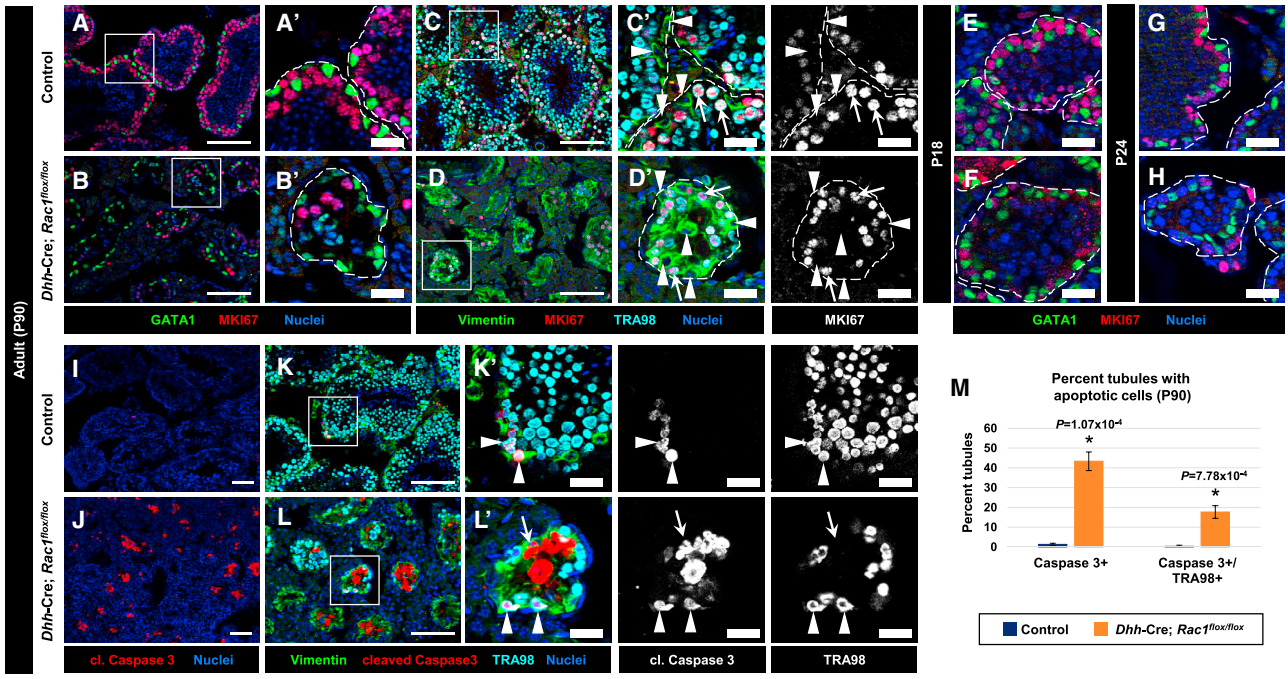

Figure 2. Cell-Cycle Status and Onset of Sertoli Cell Quiescence Is Normal in *Rac1* cKO Testes

(A–L) Three-month-old (P90) (A–D, I–L), P18 (E and F), and P24 (G and H) control *Dhh*-Cre;*Rac1*$^{flox/+}$ (A, C, E, G, I, and K) and *Dhh*-Cre;*Rac1*$^{flox/flox}$ cKO (B, D, F, H, J, and L) testes. (A)–(D'), (K'), and (L') are higher-magnification images of the boxed regions in (A)–(D), (K), and (L).

(A and B) Both P90 control (A) and cKO (B) GATA1^{+} Sertoli cells are negative for MKI67.

(C and D) While vimentin^{+} Sertoli cells are MKI67^{-} (arrowheads), TRA98^{+} germ cells are MKI67^{+} (arrows) in both control (C) and cKO (D) testes.

(E–H) Both control (E and G) and cKO (F and H) Sertoli cells are MKI67^{-} at P18 (E and F) and P24 (G and H).

(I and J) Relative to controls (I), cKO testes (J) show an increase in cell death within tubules.

(K and L) While virtually all of the apoptotic cells in control testes (K) are TRA98^{+} germ cells (arrowheads), some vimentin^{+} Sertoli cells are apoptotic in cKO (L) tubules (arrow in L). Dashed outlines indicate tubule boundaries. Thin scale bar, 100 μm; thick scale bar, 25 μm.

(M) Average percentage of tubules containing cleaved caspase 3^{+} cells or cleaved caspase 3/TRA98^{++} cells in P90 control versus cKO testes (n = 50 tubules each from 3 independent males).

The data are represented as means ± SDs. p values were performed via a two-tailed Student's t test.

it was difficult to detect apoptotic cells expressing either GATA1 or GATA4 (i.e., Sertoli cells), possibly due to rapid protein degradation during apoptosis in Sertoli cells; while this protein degradation precluded the ability to assess the rate of Sertoli cell apoptosis definitively, it is likely that there was significant apoptosis of Sertoli cells in cKO testes.

Rac1 Function Is Required for the Progression of Adult Spermatogenesis

To determine whether germ cell death was due to a failure to differentiate, we assessed spermatogenesis in adult *Dhh*-Cre; *Rac1*$^{flox/flox}$ cKO males, and observed severe defects. At 3 months of age, there was a dramatic reduction in germ cell number, with 20% of tubules being Sertoli-cell-only tubules in cKO testes (n = 3 independent males, 25 tubules each) and other tubules with a severe reduction in germ cell number (see Figure 1B and quantification in Figure 3K). To address how the loss of Sertoli *Rac1* influenced germ cell development, we examined spermatogenic cell types in cKO testes. Undifferentiated spermatogonia, as labeled by GFRA1 and ZBTB16 (also known as PLZF), were observed in cKO testes (Figures 3A–3F). GFRA1^{+} cells were present at slightly higher numbers in cKO tubules that contained GFRA1^{+} cells (Figure 3L), and were always observed in their normal basal location (Figures 3A and 3B).

To determine whether undifferentiated spermatogonia could transition into A1 differentiating spermatogonia, we used the marker STRA8, which turns on at lower levels starting in differentiating spermatogonia (Zhou et al., 2008), and co-expresses along with low levels of ZBTB16 (Figures 3C–3F). STRA8 was present at higher levels in preleptotene spermatocytes, and STRA8-bright cells were found in a subset of tubules in cKO testes as in control testes (Figures 3C–3F). Quantification of STRA8^{+} cells in adult (P90) testes revealed a similar percentage of tubules with STRA8^{+} cells in cKO testes (19.0% ± 7.1% tubules in controls versus 29.5% ± 11.5% tubules in cKO testes; n = 3 independent males, 35 tubules each; p = 0.253).

We next examined γH2AX (official name: H2AFX), which is expressed diffusely in leptotene spermatocytes and gradually becomes restricted and enriched in the XY sex body by pachytene stages, as well as H1T (official name: HIST1H1T), a testis-specific linker histone that appears during pachytene stages and is maintained through round spermatid stages. We observed both γH2AX^{+} cells and H1T^{+} cells throughout adult cKO testes (Figures 3G–3J), and found that γH2AX was enriched in the XY

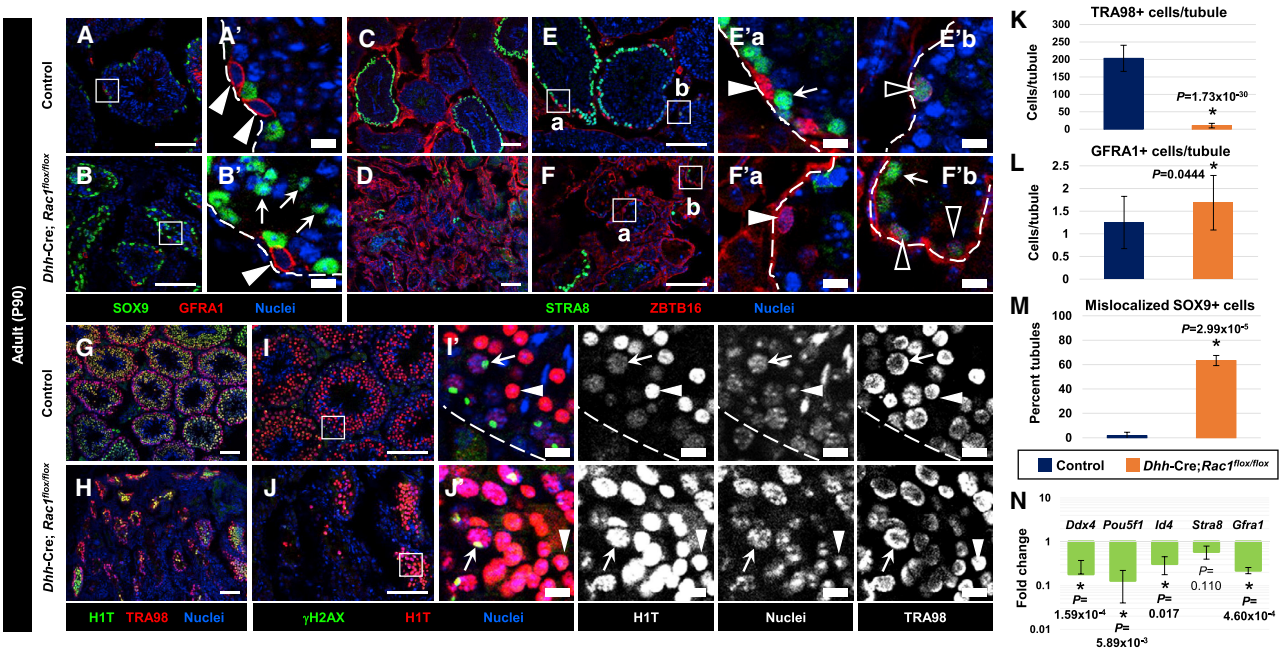

Figure 3. *Rac1* Function in Sertoli Cells Is Required for Later Stages of Adult Spermatogenesis

(A–J) Three-month-old (P90) control (*Dhh*-Cre;*Rac1*$^{flox/+}$) (A, C, E, G, and I) and *Dhh*-Cre;*Rac1*$^{flox/flox}$ cKO (B, D, F, H, and J) testes. (A'), (B'), (E'), (F'), (I'), and (J') are higher-magnification images of the boxed regions in (A), (B), (E), (F), (I), and (J). Dashed outlines indicate tubule boundaries.

(A and B) GFRA1^{+} undifferentiated spermatogonia (arrowheads) are at a basal location in both control (A) and cKO (B) tubules, while cKO Sertoli cells are often observed in the center of tubules (arrows in B').

(C–F) ZBTB16-bright/STRA8^{-} undifferentiated spermatogonia (white arrowheads in E' and F'), ZBTB16-dim/STRA8-dim differentiating spermatogonia (black arrowheads in E' and F'), and ZBTB16^{-}/STRA8-bright spermatocytes (arrows in E' and F') are present in both control (C and E) and cKO (D and F) testes.

(G and H) H1T^{+} meiotic and post-meiotic cells are visible in cKO testes (H), although in reduced numbers relative to controls (G).

(I and J) γH2AX/H1T^{++} spermatocytes with XY-body-enriched γH2AX staining (arrows) and H1T-bright round spermatids (arrowheads) are observed in both control (I) and cKO (J) tubules. Thin scale bar, 100 μm; thick scale bar, 10 μm.

(K) Average number of TRA98^{+} germ cells per tubule in P90 control versus cKO (n = 3 tubules each from 3 independent control males and n = 15 tubules each from 3 independent cKO males).

(L) Average number of GFRA1^{+} cells per tubule in germ cell-containing tubules in P90 control versus cKO testes (n = 25 tubules each from 3 independent males).

(M) Average percentage of tubules displaying SOX9^{+} Sertoli cells mislocalized within the tubule lumen in P90 control versus cKO testes (n = 20 tubules each from 3 independent control males and n = 50 tubules each from 3 independent cKO males).

(N) Quantitative real-time PCR analyses showing reduction in germ cell gene expression in P90 cKO testes relative to controls (n = 3 testes, each from independent males).

The data in (K)–(N) are shown as means ± SDs. p values were performed via a two-tailed Student's t test.

sex body of spermatocytes (Figure 3J). Nuclear morphology and H1T expression also revealed that round spermatids were regularly found in cKO testes (Figure 3J). However, elongating and condensing spermatids (as determined by nuclear morphology) were never observed in the tubules of cKO mice. Quantitative real-time PCR analyses revealed that germ cell gene expression was significantly decreased in cKO testes (Figure 3N), as mRNA levels were reduced for genes expressed in undifferentiated spermatogonia (*Pou5f1* [also known as *Oct4*], *Gfra1*, and *Id4*), differentiating spermatogonia, and preleptotene spermatocytes (*Stra8* and *Ddx4* [also known as *Mvh*]), and later spermatocyte stages (*Ddx4*).

Rac1 cKO Males Exhibit Disruptions in FSH and Inhibin B Hormone Production

We next determined whether disruptions in spermatogenesis or Sertoli cell function were due to or resulted in defects in hormone production (Figure S2). We found no change in protein or mRNA levels of steroidogenic enzymes such as *Cyp11a1* and *Cyp17a1* at P7, but there was increased *Cyp11a1* expression at P90 in cKO testes, likely due to an increased relative proportion of Leydig cells in adult cKO testes (as mentioned above). We also measured levels of testosterone (T), luteinizing hormone (LH), and FSH in 3- to 4-month-old cKO mice; however, we did not observe any significant changes in the levels of these hormones at this age (Figure S2G).

While we saw no statistically significant differences in T, LH, and FSH levels at 3–4 months, there were some disruptions in 6- to 7-month-old testes. We saw a slight, statistically significant decrease in T levels (~30% reduction) at 6–7 months of age, but there was no change in testicular or serum LH levels at 6–7 months, suggesting that there was minimal, if any, disruption in systemic T signaling. In contrast, we saw a significant, more severe (~65%–70%) reduction in FSH levels at 6–7 months in

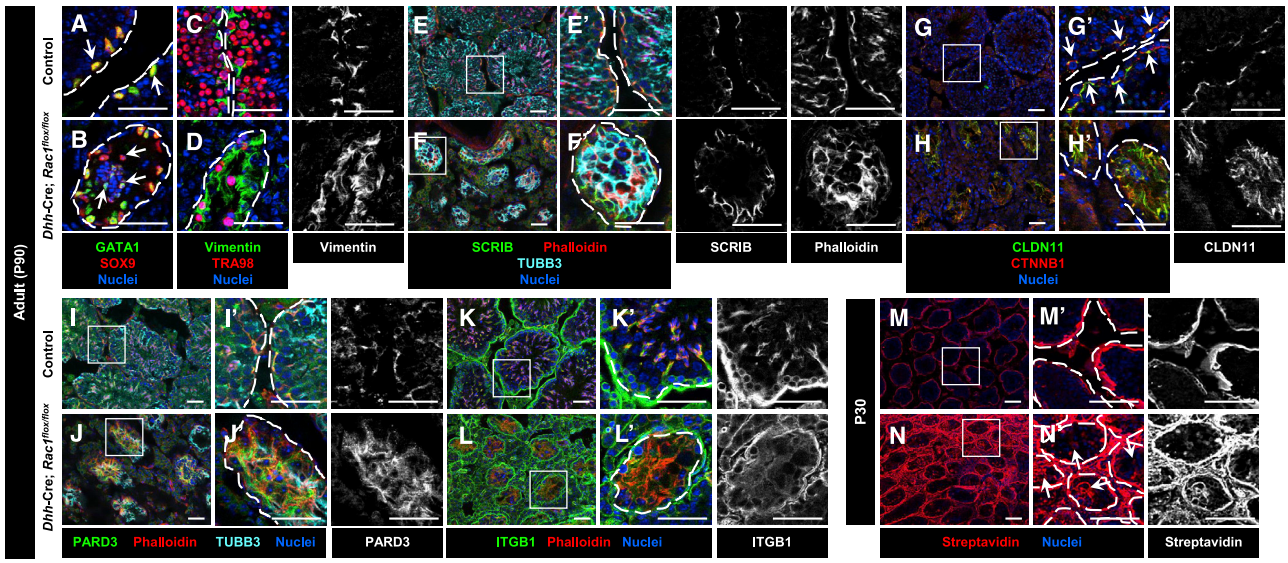

Figure 4. Apicobasal Cell Polarity and BTB Are Disrupted in Adult *Rac1* cKO Sertoli Cells

(A–N) Three-month-old (P90) (A)–(L) and 1-month-old (P30) (M and N) control *Dhh*-Cre;*Rac1*$^{flox/+}$ (A, C, E, G, I, K, and M) and *Dhh*-Cre;*Rac1*$^{flox/flox}$ cKO (B, D, F, H, J, L, and N) testes. (E')–(N') are higher-magnification images of the boxed regions in (E)–(N). Dashed outlines indicate tubule boundaries.

(A and B) GATA1^{+}/SOX9^{+} Sertoli cell nuclei (arrows) in controls (A) are localized basally, but cKO nuclei (B) are both basally and centrally localized within the tubule.

(C and D) Relative to controls (C), Vimentin is localized ectopically throughout the entire cKO Sertoli cell (D).

(E and F) SCRIB is localized to the BTB and basal Sertoli compartment in both control (E) and cKO (F) testes. However, phalloidin staining is localized ectopically throughout the entire cKO Sertoli cell (see also I–L).

(G and H) CLDN11 and CTNNB1 are enriched in a specific ring-like network (BTB; arrows in G') in control Sertoli cells (G), but they are localized throughout the entire cKO Sertoli cell (H).

(I and J) PARD3 is normally enriched at the BTB and apical ES in controls (I), but it is localized throughout the entire cKO Sertoli cell (J). Note that PARD3 is also localized to the BTB.

(K and L) ITGB1 is localized diffusely throughout cKO tubules (L), in contrast to specific apical ES staining in controls (K); however, basement membrane, spermatogonial, and interstitial staining is still observed in both control and cKO testes.

(M and N) One-month-old (P30) control (*Dhh*-Cre;*Rac1*$^{flox/+}$) (M) and cKO (N) testes injected with biotin (and detected with streptavidin). cKO testes showed widespread infiltration of biotin deep into tubule lumens (arrows). Scale bar, 50 μm.

See also Figure S4.

cKO testes. Finally, we measured the levels of the Sertoli-produced hormone inhibin B and found that serum levels were significantly reduced at both 3–4 months (~80%–85% reduction) and 6–7 months (~85%–90% reduction) in cKO males (Figure S2G).

We also assessed the expression of other Sertoli-expressed paracrine signaling factors and nuclear factors in cKO testes via quantitative real-time PCR analyses. In P90 cKO testes, we found that *Sox9* and *Ar* were upregulated, while *Inhbb*, *Dhh*, *Gdnf*, *Fshr*, *Pdgfa*, and *Gata1* expression were unaffected (Figure S3A). However, after normalization to *Sox9* to account for changes in Sertoli cell contributions to the testis after germ cell loss, we found that the expression of *Inhbb*, *Dhh*, *Gdnf*, *Fshr*, *Pdgfa*, and *Gata1* were reduced to 10%–25% of control levels (Figure S3B).

Rac1 Function Is Required for Apicobasal Polarity of Sertoli Cells

We next sought to determine the effects of *Rac1* deletion on Sertoli cell polarity, one aspect of which is nuclear localization within the cell. Unlike the consistent basal localization seen in control Sertoli cells, cKO Sertoli cell nuclei (SOX9^{+}/GATA1^{+}) were found in the centers of >60% of the seminiferous tubules, ranging from lone nuclei to intratubular clusters of 10–20 nuclei (Figures 4A and 4B; see also Figures 2A, 2B, 3A, 3B, and 3M). Another Sertoli-expressed protein, vimentin, is normally localized in the cytoplasm basally near the nucleus, but it was ectopically localized throughout the entire Sertoli cell in cKO testes (Figures 4C and 4D; see also Figures 2C and 2D). A component of the basal polarity protein complex, SCRIB, was expressed in the basal domain of the Sertoli cell near to and along the BTB in control testes. SCRIB localization was not altered in cKO testes (Figures 4E and 4F). As an additional marker of the BTB and to highlight the basal and apical ES, we used phalloidin to label F-actin. F-actin localization in cKO testes was severely disrupted, with phalloidin brightly staining throughout the entire tubule, as opposed to the specific ES and BTB staining in control tubules (Figures 4E, 4F, and 4I–4L). Two additional markers of the BTB, CTNNB1 (β-catenin) and CLDN11 (Claudin 11) were dramatically mislocalized within cKO Sertoli cells, as they were expressed throughout the cells (Figures 4G and 4H). Finally, two apical markers of Sertoli cells, PARD3 (Par3) and ITGB1 (β1-integrin),

were disrupted in cKO Sertoli cells and were mislocalized diffusely throughout the cell (Figures 4I–4L).

To determine whether the disruption of polarity proteins in cKO testes resulted in a functionally compromised BTB, we tested barrier function via a biotin tracer assay, in which a large-molecular-weight tracer was injected into the interstitium of the testis. At P30, at which point BTB integrity should be well established, we observed the biotin tracer in control testes only within the interstitial compartment and in the basal-most layer of spermatogenic cells (i.e., spermatogonia) in certain tubules (Figure 4M). However, in cKO testes, we observed widespread tracer penetration into the center of tubules (Figure 4N), indicating that the BTB was functionally disrupted.

To assess whether any of the observed changes in cKO Sertoli cells were merely due to the loss of germ cells, we examined a number of Sertoli and polarity markers in two mouse models of germ cell deficiency, *Dnd1*$^{Ter/Ter}$ and *Kit*^{W}/*Kit*$^{W\text{-}v}$. On a C57BL/6J background, *Dnd1*$^{Ter/Ter}$ mutant mice exhibit a complete loss of germ cells, with no teratoma formation, while *Kit*^{W}/*Kit*$^{W\text{-}v}$ mutants possess a reduced number of undifferentiated spermatogonia, but no differentiated germ cells. Sertoli cell phenotypes in both germ cell-deficient models were similar: the BTB marker CLDN11 and the basal marker SCRIB were normally localized, but the BTB marker CTNNB1 and the apical marker PARD3 were mislocalized throughout the entire Sertoli cell (Figure S4). However, we saw that GATA1^{+} Sertoli cell nuclei were in their normal basal location and that AR protein was largely localized to the Sertoli cell nucleus, although not as strongly as in control testes (Figure S4). These findings suggest that most Sertoli defects in *Rac1* cKO testes cannot be attributed solely to a loss of germ cells.

Rac1 Sertoli Function Is Not Required for the Maintenance of Undifferentiated Spermatogonia

To determine whether SSCs or transit-amplifying undifferentiated spermatogonia were maintained by *Rac1* cKO Sertoli cells, we examined 7-month-old cKO testes, as by this point, defective SSCs or progenitors would lead to a loss in steady-state spermatogenesis; for example, *Zbtb16* mutant (*Plzf* mutant) testes, which have defects in SSC maintenance and proliferation of transit-amplifying progenitors, show a severe loss in germ cells more clearly at 6 months of age as compared to younger mice (Buaas et al., 2004; Costoya et al., 2004). We observed that TRA98^{+} germ cells were still present in 7-month-old *Rac1* cKO testes (Figures 5A and 5B). We specifically examined undifferentiated spermatogonia and regularly observed these cells in cKO testes, comparably to controls and in the normal basal position within cKO tubules (Figures 5C–5F). We also examined markers of differentiating spermatogonia (KIT and STRA8) and spermatocytes (STRA8 and DDX4) and found these germ cell types in cKO testes, although as expected, in fewer numbers relative to controls (Figures 5G–5L). Finally, H1T staining revealed cells only up to the round spermatid stage in cKO testes (Figures 5M and 5N), similar to what we observed at 3 months of age.

Germ Cell and Sertoli Cell Death in cKO Testes Precedes BTB Disruption

We next investigated when defects in testicular development began in cKO testes. We examined testes at P24, a stage at which the BTB has been established for at least 1 week and meiotic cells are widespread in the seminiferous epithelium. We observed occasional patches of germ cell loss already in P24 cKO testes (Figures S5A and S5B), which resulted in the vacuolization of Sertoli cells within tubules and a 40% reduction in tubule cross-sectional area (Figure S5I). cKO testes at this stage already exhibited a reduction in the number of Sertoli cells per tubule (Figure S5J) and a large increase in the number of tubules with Sertoli cell nuclei mislocalized to the lumen (Figure S5K). However, we did not observe any reduction in the percentage of tubules containing GFRA1-expressing spermatogonia in cKO testes (30.7% ± 10.1% tubules in controls versus 41.3% ± 6.1% tubules in cKO testes; n = 3 independent males, 25 tubules each; p = 0.192), and saw a slight increase in the number of GFRA1^{+} cells per tubule within those tubules in cKO testes (Figure S5L).

As for Sertoli cells, AR protein in P24 cKO Sertoli cells was localized throughout the entire cell, unlike the nuclear localization observed in control testes (Figures S5C and S5D). Examination of AMH expression revealed similar levels of expression in cKO and control testes (Figures S5E and S5F). There were common irregularities of the BTB in cKO testes, such as aggregates of CLDN11 in the center of the tubule (Figures S5G and S5H), suggesting that the BTB structure is already disrupted in P24 cKO testes. Roughly 40% of tubules in cKO testes contained cleaved caspase 3^{+} cells (Figure S5M); cell death appeared to occur less frequently in germ cells than in somatic cells (Figure S5M), suggesting that Sertoli cells likely make up the majority of apoptotic cells in P24 cKO testes.

We next looked at an earlier postnatal stage, P7, to assess whether there were any earlier defects in *Rac1* cKO testes. The tubule area was unchanged between control and cKO testes, and we did not see any overt disruptions in spermatogenesis, as there were no reductions in germ cell number, protein expression, or mRNA levels (in either undifferentiated or differentiating spermatogonia) (Figures 6A–6D, and 6O–6Q). However, we did observe a decrease in AMH and GATA1 protein expression in Sertoli cells via immunofluorescence (although quantitative real-time PCR did not reveal any significant change in *Amh* or *Gata1* mRNA levels), in addition to a 25% reduction in the number of SOX9^{+} Sertoli cells (Figures 6E–6H, 6O, and 6P). This reduction in Sertoli cell number could be due to an increase in cell death, as seen by GATA4^{+} cells expressing cleaved caspase 3 (Figures 6I–6L); consistent with this finding, quantifications indicated that most of the apoptotic cells in tubules were TRA98^{-} (Figure 6R). Despite being the minority of apoptotic cells, germ cells were also undergoing cell death at an increased rate in cKO testes (Figures 6K, 6L, and 6R); however, we did not see any decreases in DDX4^{+} germ cell number at this stage (Figure 6P). We also observed that the radial migration of germ cells to the basement membrane was normal in cKO tubules (Figures 6A–6D), and we saw a slight increase in the number of GFRA1^{+} cells per tubule (Figure 6P). Consistent with these results, cell-cycle status (as visualized by MKI67 expression) was normal in both germ and Sertoli cells in cKO testes as compared to controls (Figures 6M and 6N).

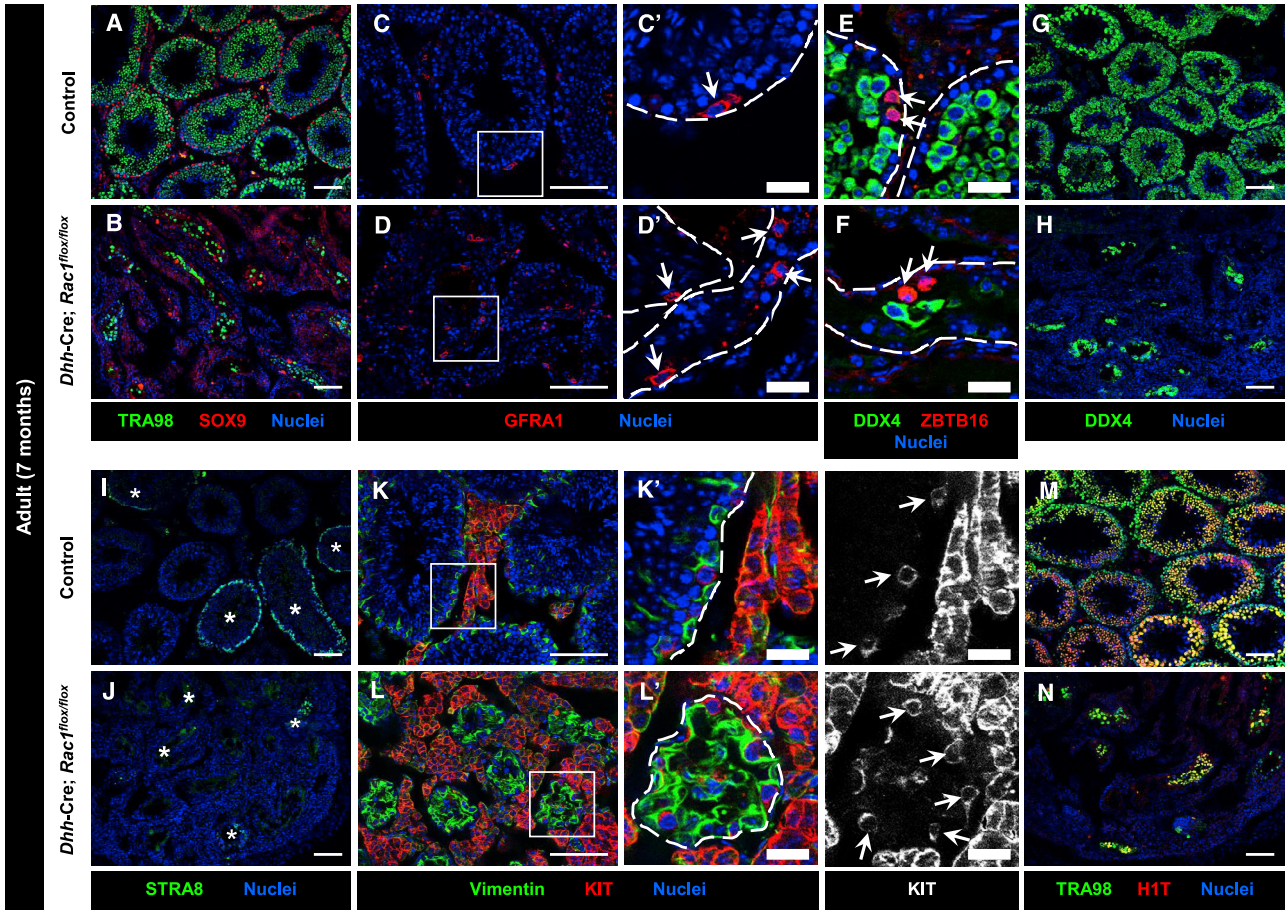

Figure 5. *Rac1* Function in Sertoli Cells Is Dispensable for the Maintenance of Undifferentiated Spermatogonia

(A–N) Seven-month-old control *Dhh*-Cre;*Rac1*$^{flox/+}$ (A, C, E, G, I, K, and M) and *Dhh*-Cre;*Rac1*$^{flox/flox}$ cKO (B, D, F, H, J, L, N) testes. (C'), (D'), (K'), and (L') are higher-magnification images of the boxed regions in (C), (D), (K), and (L). Dashed outlines indicate tubule boundaries.

(A and B) Relative to controls (A), cKO testes (B) have smaller tubules, containing a variable number of TRA98^{+} germ cells.

(C–H) Similar to controls (C, E, and G), cKO testes (D, F, and H) still have GFRA1^{+} and ZBTB16^{+} undifferentiated spermatogonia within tubules (arrows in C–F); cKO testes also contain a variable number of DDX4^{+} germ cells, albeit in reduced numbers.

(I–L) As in controls (I and K), cKO testes (J and L) contain STRA8^{+} differentiating spermatogonia and spermatocytes (asterisks in I and J), as well as KIT^{+} differentiating spermatogonia (arrows in K' and L').

(M and N) Relative to controls (M), cKO tubules (N) have a reduced, variable number of H1T^{+} spermatocytes and round spermatids. Thin scale bar, 100 μm; thick scale bar, 25 μm.

Immune Cells Infiltrate into Postnatal cKO Tubules

One potential consequence of disrupted Sertoli cell barrier function is the increased infiltration of immune cells into the testis and, in particular, into the interior of seminiferous tubules. We observed in adult cKO testes that there was a significant increase in CD45^{+} cells, mostly AIF1^{+} (IBA1^{+}) macrophages (Figures S6A–S6D). However, in cKO testes, there was also an increase in CD45-bright cells, which were CD4^{+} T cells (Figures S6E and S6F), and were rarely observed in control testes. We also observed an increase in immune cell infiltration into cKO tubules at P7 and P24 (Figures S6G–S6L), although at P7, there was no observable difference in total CD45^{+} immune cell numbers (Figures S6I and S6J). Quantification revealed that immune cells were never found inside the tubules of control testes at P7, P24, and P90, but they were observed in 11%, 18%, and 26% of tubules in cKO tubules at those stages, respectively (Figure S6N). When macrophages were inside tubules, they were rounder and larger than interstitial macrophages and were often observed engulfing both germ and Sertoli cells (Figure S6M).

Apicobasal Cell Polarity Is Not Yet Fully Established in the Fetal Testis

While previous studies showed that certain markers of adult Sertoli polarity, such as CTNNB1, are expressed in Sertoli cells in late fetal stages (Chang et al., 2008), it is not clear whether polarity proteins have specific subcellular localization in the fetal testis. We examined markers of cell polarity in the fetal testis and saw that a subset of apicobasal polarity genes, such as *Rac1*, *Pard3* (*Par3*), *Scrib* (*Scribble*), and *Pard6a*

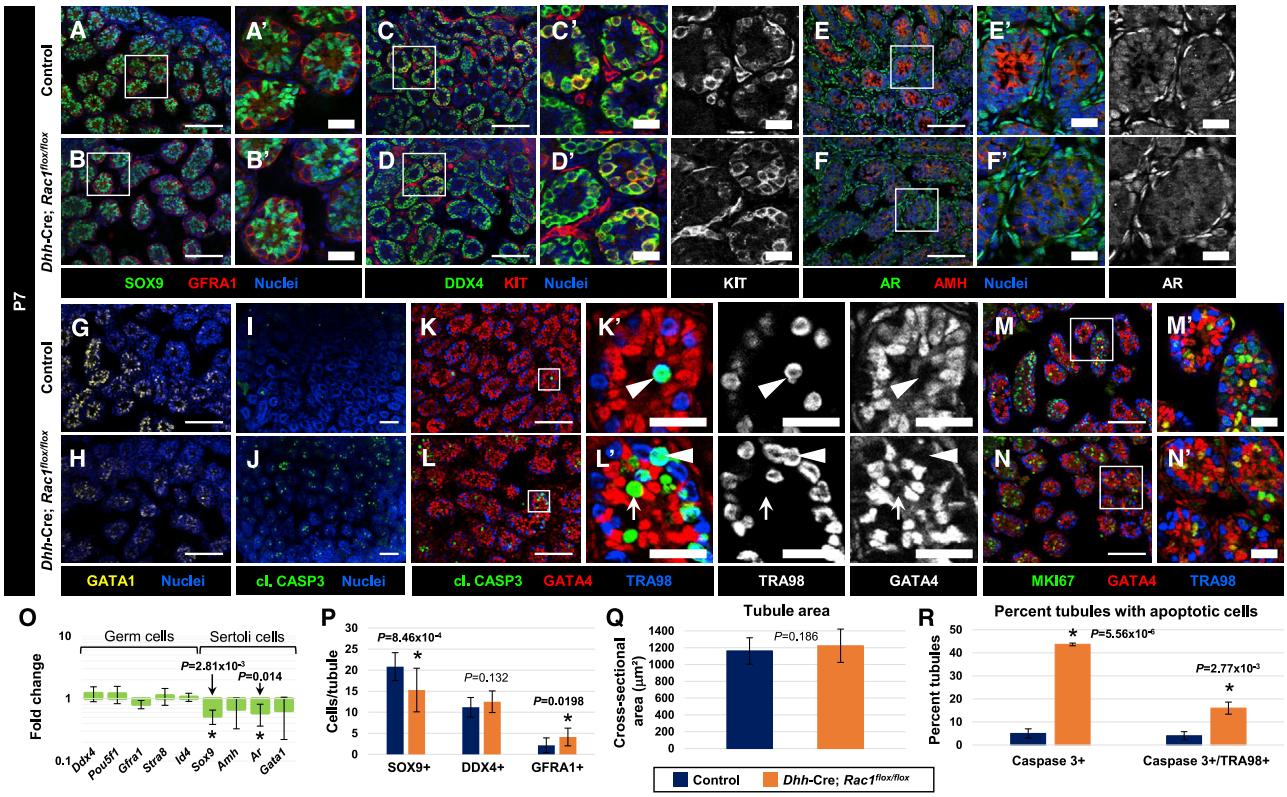

Figure 6. Sertoli *Rac1* Function Is Largely Dispensable for Postnatal Testicular Development

(A–N) P7 control *Rac1*$^{flox/flox}$ (A, C, E, G, I, K, and M) and *Dhh*-Cre;*Rac1*$^{flox/flox}$ cKO (B, D, F, H, J, L, and N) testes. (A')–(F') and (K')–(N') are higher-magnification images of the boxed regions in (A)–(F) and (K)–(N).

(A–D) As in controls (A and C), P7 cKO testes (B and D) possess SOX9^{+} Sertoli cells, GFRA1^{+} undifferentiated spermatogonia, and DDX4^{+}/KIT^{+} differentiating spermatogonia. Germ cells in cKO testes, similar to controls, have migrated to the tubule periphery.

(E–H) Compared to controls (E and G), P7 cKO testes (F and H) express slightly lower levels of AMH, less nuclear AR in Sertoli cells (although interstitial expression and nuclear localization are normal), and slightly lower levels of GATA1.

(I and J) Relative to controls (I), a significant increase in apoptosis is observed in cKO tubules (J).

(K and L) Apoptosis is observed in mostly TRA98^{+} germ cells (arrowheads) in controls (K), but it is also observed in Sertoli cells (arrows) in cKO testes (L).

(M and N) Most Sertoli and germ cells in both controls (M) and cKO tubules (N) are MKI67^{+}. Thin scale bar, 100 μm; thick scale bar, 25 μm.

(O) Quantitative real-time PCR analyses reveal no difference in germ cell gene expression in P7 control versus cKO testes (*Ddx4*, *Pou5f1*, *Gfra1*, *Stra8*, and *Id4*), but they do reveal a significant reduction in the Sertoli-expressed genes *Sox9* and *Ar*, with no significant change in *Amh* and *Gata1* expression (n = 4–6 testes for controls and cKO, each from independent males).

(P) Graph showing slightly reduced Sertoli cell numbers in P7 cKO testes, but no loss of either DDX4^{+} or GFRA1^{+} germ cells (n = 10 tubules each from 3 testes, each testis from independent males).

(Q) Average tubule cross-sectional area of P7 control versus cKO testes (n = 10 tubules each from 3 independent males).

(R) Average number of tubules with CASP3^{+} cells and CASP3^{+}/TRA98^{+} germ cells in P7 control versus cKO testes (n = 50 tubules each from 3 independent males). The data in (O)–(R) are shown as means ± SDs. p values were calculated using a two-tailed Student's t test.

See also Figures S5 and S6.

(*Par6*), were either expressed in the fetal testis ubiquitously (i.e., not specifically in Sertoli cells) or not at all (Figures S1A, and S7A–S7C), unlike other well-characterized Sertoli-specific genes (e.g., *Dhh*; see Figure S1B). At the protein level, cell polarity complex proteins such as PARD3 and SCRIB were not localized apicobasally in fetal Sertoli cells at either early (E13.5) or late (E18.5) fetal stages of testis differentiation, and instead, were localized throughout the entire Sertoli cell (Figures S7D–S7G). Therefore, it seems that cell polarity complexes are not yet specifically localized in fetal Sertoli cells.

Rac1 Sertoli Function Is Dispensable for Fetal Testis Differentiation

To determine whether Sertoli *Rac1* function is required for fetal testis differentiation, we examined several parameters of Sertoli and germ cells in E18.5 control and cKO fetal testes. We saw that cKO tubules had a similar size, structure, and number of SOX9^{+} Sertoli cells per tubule as compared to controls (Figures 7A, 7B, and 7M). Leydig cell development and male-specific vascularization of the testis, which are driven indirectly by Sertoli cells, were also normal in cKO testes (Figures 7C and 7D). We did see a significant increase in the amount of cell death in cKO

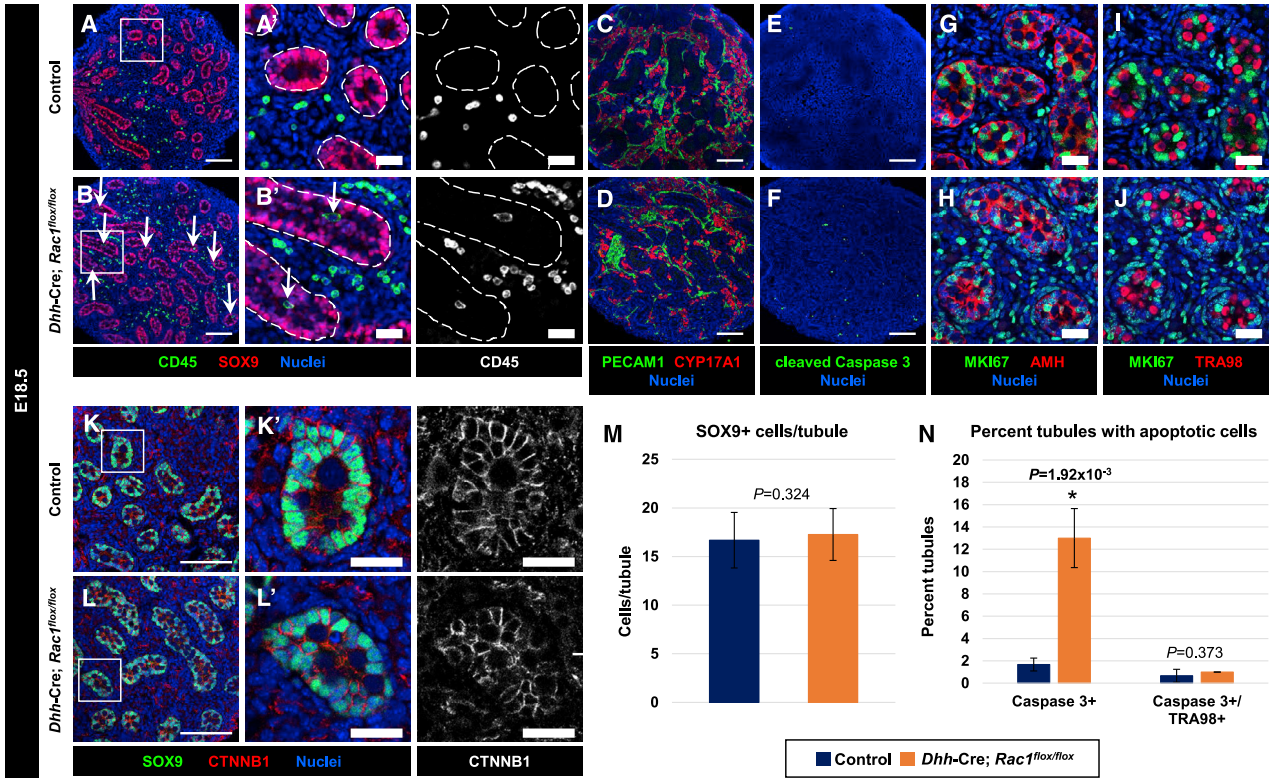

Figure 7. Sertoli *Rac1* Function Is Dispensable for Fetal Testis Differentiation

(A–L) E18.5 *Rac1*$^{flox/flox}$ control (A, C, E, G, I, and K) and *Dhh*-Cre;*Rac1*$^{flox/flox}$ cKO (B, D, F, H, J, and L) fetal testes. (A'), (B'), (K'), and (L') are higher-magnification images of the boxed regions in (A), (B), (K), and (L). Dashed lines indicate tubule boundaries.

(A and B) Both control (A) and cKO (B) tubules exhibit normal morphology and presence of SOX9^{+} Sertoli cells. CD45^{+} immune cells are observed within tubules in cKO testes (arrows in B and B').

(C and D) Both control (C) and cKO (D) testes show normal vascularization (PECAM1^{+} cells) and Leydig cell development (CYP17A1^{+} cells).

(E and F) Relative to controls (E), cKO testes (F) exhibit an increase in apoptosis (cleaved caspase 3^{+} cells).

(G–J) Both control (G and I) and cKO (H and J) tubules contain MKI67^{+} Sertoli cells (AMH^{+}) and MKI67^{-} germ cells (TRA98^{+}).

(K and L) Control (K) and cKO (L) tubules show similar expression of CTNNB1. Thin scale bar, 100 μm; thick scale bar, 25 μm.

(M) Cell counts of SOX9^{+} cells per tubule in control versus cKO E18.5 testes (n = 15 tubules each from 3 independent males).

(N) Average percentage of tubules containing cleaved caspase 3^{+} cells or cleaved caspase 3/TRA98^{++} cells in control versus cKO E18.5 testes (n = 50 tubules each from 3 independent males).

The data in (M) and (N) are shown as means ± SDs. p values were calculated using a two-tailed Student's t test.

See also Figure S7.

testes, which quantifications revealed occurred almost exclusively in Sertoli cells (Figures 7E, 7F, and 7N); however, this increase in cell death did not appear to affect testicular development. In cKO testes, germ cells were in cell-cycle arrest (as evidenced by MKI67 immunonegativity), similar to control germ cells, and cKO Sertoli cells maintained active cell-cycle status (MKI67 immunopositivity) and strong AMH expression, similar to controls (Figures 7G–7J). We also saw that the expression of CTNNB1 in tubules was similar between cKO and control testes (Figures 7K and 7L). We observed CD45^{+} immune cells within tubules in cKO testes more often than controls (Figures 7A and 7B), likely due to an increase in cell death in tubules; however, this difference was not statistically significant (Figure S6N), as a small percentage of control tubules also contained immune cells at E18.5. Furthermore, there did not appear to be an overall increase in the number of CD45^{+} immune cells in fetal cKO testes (Figures 7A and 7B). Overall, we found that Sertoli *Rac1* function was dispensable for fetal aspects of testicular and germ cell development.

DISCUSSION

In this study, we definitively demonstrate that Sertoli cells require *Rac1* function for the normal progression of spermatogenesis to occur, which we propose is due to the role of *Rac1* in establishing apicobasal polarity. By conditionally deleting *Rac1* in Sertoli cells, we aimed to address the importance of apicobasal cell polarity at distinct stages of testicular development and spermatogenesis. Consistent with previously characterized roles for *Rac1* in cell polarity in other contexts, the disruption of Sertoli *Rac1* expression had a significant impact on testicular structure and function in adult stages. The most apparent was the dramatic decrease in testis weight and seminiferous tubule size due to the decreased number of germ cells, along with a decrease in

the number of Sertoli cells. Germ cells were still present in cKO animals, in particular, undifferentiated spermatogonia, but their overall numbers were diminished. Specifically, there were no elongating spermatids or later spermatogenic stages in cKO testes, demonstrating that complete spermatogenic arrest occurred at the round spermatid stage. Consequently, adult cKO males were azoospermic. Overall, our data show that although *Rac1* function in adult Sertoli cells is required for later stages of spermatogenesis and spermiogenesis, it is dispensable for the establishment and maintenance of undifferentiated spermatogonia and for fetal testis differentiation.

The proteins responsible for BTB structure and apicobasal polarity were examined in cKO testes, and we found that while virtually all of the apical proteins observed were significantly mislocalized, SCRIB, a basally located complex, retained normal localization. The disruption of these apical polarity complex proteins, along with the disperse localization of F-actin, could serve as explanation for the loss of the elongating spermatids observed in cKO testes, since the cellular architecture may be compromised and unable to sustain and tether germ cells to the seminiferous epithelium. Alternatively, these proteins are normally present in structures associated with elongating and condensing spermatids that are never observed in cKO testes, and therefore, mislocalization of these proteins may be a secondary effect caused by the absence of late-stage spermatid populations. However, the intact localization of SCRIB suggests *Rac1* is at least dispensable for its expression and localization, but it is necessary for the regulation of other major polarity complexes. This finding suggests that the basal compartment of the Sertoli cell retained some identity in cKO Sertoli cells and that this residual basal Sertoli identity was sufficient to maintain stem-progenitor spermatogenic cells in cKO testes and localize them to the basement membrane.

While some Sertoli function may remain due to some residual basal identity of cKO Sertoli cells, it is also possible that interstitial cells could compensate for disrupted Sertoli cell function in promoting at least some aspects of spermatogenesis, as interstitial cells of different lineages (e.g., immune cells, vasculature, peritubular cells) have been implicated in testicular differentiation, spermatogenesis, and activity of the SSC niche (Heinrich and DeFalco, 2019; Potter and DeFalco, 2017). Cytokines and growth factors such as GDNF (Chen et al., 2014; Chen et al., 2016) secreted by these interstitial cells may work in concert with Sertoli cells and perhaps even compensate when Sertoli cell function is disrupted, in an attempt to maintain spermatogenesis and fertility.

Considering that *Rac1* is expressed in Sertoli cells as early as E11.5, we were surprised to observe relatively normal testicular structure and function in fetal and early postnatal cKO testes. At P7, there were some early signs of altered Sertoli cell function (e.g., reduced *Sox9* and *Ar* mRNA levels) and an increase in apoptotic cells, yet overall germ cell numbers, cell-cycle status, and tubule size were not affected. At E18.5, even fewer distinctions were observed between control and cKO testes. These findings are supported by our investigation into the expression of polarity complexes at embryonic time points. While fetal Sertoli cells appear to localize their nuclei and express several polarity complex proteins, these complexes do not demonstrate any specific subcellular localization during fetal stages. Therefore, our studies suggest that *Rac1* function and, potentially, apicobasal polarity are largely inconsequential during fetal stages. It is possible that the loss of polarity only begins to affect testicular development during the postnatal stages, when polarity is more critically required to accommodate the simultaneous presence of early- and late-stage spermatogenic cells. Our findings in P24 and P30 cKO testes support this idea, as we observed significant germ cell loss and tubule vacuolization, in addition to disruptions of nuclear AR localization and functional disruption of the BTB, at those stages.

In addition to cell polarity, it is equally important to discuss other aspects of Sertoli cell function in cKO testes. The disruption of Sertoli cell number, gene expression, or hormone production could contribute to some aspects of the disrupted testicular development and spermatogenic arrest that are observed in cKO animals. For example, non-nuclear localization of AR has been associated with the increased apoptosis of germ cells (Hill et al., 2004). Our data suggest that androgen signaling is only partly disrupted due to aberrant AR subcellular localization in *Rac1* cKO testes, since Sertoli-specific *Ar* knockout (SCARKO) mice cannot complete meiosis (Chang et al., 2004; De Gendt et al., 2004), but *Rac1* cKO testes can produce post-meiotic round spermatids. While our data did not indicate any major defects in the T-LH signaling axis, there were large reductions in FSH and inhibin B levels. It is possible that these defects are symptoms, rather than causes, of testicular defects seen in cKO testes, since *Fshb*-deficient or *Inhbb*-deficient males are fertile and have qualitatively normal spermatogenesis (Kumar et al., 1997; Vassalli et al., 1994); however, one caveat is that the reduction of FSH in *Fshb*-deficient mice does impair the capacity of individual Sertoli cells to support a large number of germ cells (Wreford et al., 2001). Furthermore, inhibin B levels respond to the presence of different germ cell populations and are sometimes reduced as a consequence, rather than as a cause, of arrested spermatogenesis (Hedger and Winnall, 2012; Meachem et al., 2001). Therefore, it is unlikely that the early spermatogenic arrest in *Rac1* cKO testes is simply due to low levels of FSH or inhibin B; it is likely due to multiple defects in Sertoli cell function, initiated by defective cell polarity and cytoarchitecture downstream of *Rac1* deletion, which inhibit the completion of spermatogenesis. We additionally found that levels of several paracrine signaling factors were reduced in cKO testes, such as *Dhh*, *Gdnf*, and *Pdgfa*; however, given that testis cord morphogenesis, vascularization, Leydig cell differentiation, and SSC maintenance, which are dependent on these factors, were grossly normal, it is unlikely that any potential disruption of these paracrine signaling factors had functional consequences with regard to the development of cKO testes.

In our analysis of germ cell-depleted testes of $Dnd1^{Ter/Ter}$ and $Kit^{W\text{-}Wv}$ males, we determined that certain aspects of Sertoli cells, such as specific subcellular localization of PARD3 and CTNNB1, were disrupted, even though Sertoli cells are ostensibly unaffected, at least directly, by these particular mutations. These findings suggest that adult Sertoli cell function is at least partly regulated by germ cell feedback, similar to GATA1 expression (Yomogida et al., 1994); thus, we cannot conclude that PARD3 and CTNNB1 disruption is solely due to *Rac1* deletion. However, most aspects of Sertoli cell polarity were maintained in the absence of germ cells in these two models. Knockdown

of individual polarity complexes, possibly with genetic or small interfering RNA (siRNA) experiments, would help uncover mechanisms regulating specific Sertoli cell polarity complexes during spermatogenesis and how germ cells are important for the nucleation of polarity complexes within Sertoli cells.

In terms of potential functions for *Rac1* aside from cell polarity, our data did not support a role for Sertoli *Rac1* in regulating cell-cycle activity, which has long been proposed as a potential role of *Rac1* (Michaelson et al., 2008; Olson et al., 1995), in Sertoli or germ cells. However, Sertoli cell survival was regulated by *Rac1* to some degree, as we saw apoptosis of Sertoli cells beginning in the late fetal stages and continuing into adulthood. Further studies are required to determine whether increased cell death in cKO testes is directly or indirectly linked to disruptions in cell polarity or cytoarchitecture.

Consistent with our observance of the breakdown of the BTB beginning at ~P24–P30, we frequently noted macrophage infiltration into cKO seminiferous tubules, sometimes even in the process of phagocytosis. Phagocytic action of testicular macrophages is normally observed in the interstitial compartment of wild-type testes, but within the tubule, Sertoli cells perform the phagocytic function of clearing apoptotic germ cells (Chemes, 1986), since macrophages are excluded from the adult tubular compartment due to the functions of BTB and Sertoli cells (Meinhardt and Hedger, 2011). Increased apoptosis within cKO testes may provide an explanation for the increased incidence of macrophage infiltration in cKO tubules: the increase in apoptotic cells, along with perturbed Sertoli cell function in cKO testes, may lead to macrophages necessarily or opportunistically taking over a phagocytic role within tubules, even during fetal and early postnatal stages. It is also interesting to note that BTB structure was disrupted in cKO testes and macrophage-infiltrated tubules, but meiotic and post-meiotic germ cells were still present in 3- and 7-month-old cKO testes, suggesting that BTB activity is not solely responsible for establishing an immunosuppressive environment in the testis (Meinhardt and Hedger, 2011); perhaps some immunomodulatory function was retained in cKO Sertoli cells.

Overall, our studies have provided insight into the distinct roles of *Rac1* within Sertoli cells over the course of testicular differentiation, with a particular focus on the apicobasal polarity of Sertoli cells. While it is assumed that Sertoli cells undergo a mesenchymal-to-epithelial transition during fetal development and become polarized, our data indicate that Sertoli cells are not polarized yet at that stage, at least at the cell-intrinsic level. Only when the BTB forms and the Sertoli cell must simultaneously accommodate a wide diversity of germ cell stages does the disruption of cell polarity affect spermatogenesis or testicular function. The regulation of apicobasal polarity by *Rac1* appears to play specific roles in the adult testis, in which it is required for latter stages of spermatogenesis, but it is dispensable for most other aspects of spermatogenesis, such as maintenance of undifferentiated spermatogonia, basal localization of spermatogonia, and entry into meiosis. The distinct functions and requirements of Sertoli cell polarity, as well as the complex interactions of Sertoli cells with germ and interstitial cells, will be fruitful areas for future research and will help us understand the underlying mechanisms that drive spermatogenesis and ensure male fertility.

STAR★METHODS

Detailed methods are provided in the online version of this paper and include the following:

- KEY RESOURCES TABLE
- LEAD CONTACT AND MATERIALS AVAILABILITY
- EXPERIMENTAL MODEL AND SUBJECT DETAILS
  - Mice
- METHOD DETAILS
  - Immunofluorescence
  - Cell counts and tubule area quantification
  - RNA extraction, cDNA synthesis, and quantitative real-time PCR
  - Hormone measurements
  - Biotin tracer injections
- QUANTIFICATION AND STATISTICAL ANALYSIS
- DATA AND CODE AVAILABILITY

SUPPLEMENTAL INFORMATION

Supplemental Information can be found online at https://doi.org/10.1016/j.celrep.2020.03.077.

ACKNOWLEDGMENTS

We thank C. Moon for animal husbandry; B. Capel, D. Meijer, and Y. Zheng for providing mice; and M. Handel for the H1T antibody. We also acknowledge S.K. Dey and S.H. Namekawa for antibodies. We also thank B. Bhandary for helpful discussions, and B. Waller, C. Spinner, and M. White for preliminary experiments. This work was supported by Cincinnati Children's Hospital Medical Center funding and by National Institutes of Health grants R35GM119458 and R01HD094698 to T.D.

AUTHOR CONTRIBUTIONS

Conceptualization, A.H., S.J.P., N.R., and T.D.; Methodology, A.H., S.J.P., and T.D.; Investigation, A.H., S.J.P., L.G., and T.D.; Resources, N.R.; Writing – Original Draft, A.H. and T.D.; Writing – Review & Editing, A.H., S.J.P., N.R., and T.D.; Supervision, T.D.; Project Administration, T.D.; Funding Acquisition, T.D.

DECLARATION OF INTERESTS

The authors declare no competing interests.

Received: June 29, 2019
Revised: January 16, 2020
Accepted: March 24, 2020
Published: April 14, 2020

REFERENCES

Albrecht, K.H., and Eicher, E.M. (2001). Evidence that Sry is expressed in pre-Sertoli cells and Sertoli and granulosa cells have a common precursor. Dev. Biol. *240*, 92–107.

Buaas, F.W., Kirsh, A.L., Sharma, M., McLean, D.J., Morris, J.L., Griswold, M.D., de Rooij, D.G., and Braun, R.E. (2004). Plzf is required in adult male germ cells for stem cell self-renewal. Nat. Genet. *36*, 647–652.

Chang, C., Chen, Y.T., Yeh, S.D., Xu, Q., Wang, R.S., Guillou, F., Lardy, H., and Yeh, S. (2004). Infertility with defective spermatogenesis and hypotestosteronemia in male mice lacking the androgen receptor in Sertoli cells. Proc. Natl. Acad. Sci. USA *101*, 6876–6881.

Chang, H., Gao, F., Guillou, F., Taketo, M.M., Huff, V., and Behringer, R.R. (2008). Wt1 negatively regulates beta-catenin signaling during testis development. Development *135*, 1875–1885.

Chemes, H. (1986). The phagocytic function of Sertoli cells: a morphological, biochemical, and endocrinological study of lysosomes and acid phosphatase localization in the rat testis. Endocrinology *119*, 1673–1681.

Chen, L.Y., Brown, P.R., Willis, W.B., and Eddy, E.M. (2014). Peritubular myoid cells participate in male mouse spermatogonial stem cell maintenance. Endocrinology *155*, 4964–4974.

Chen, L.Y., Willis, W.D., and Eddy, E.M. (2016). Targeting the Gdnf Gene in peritubular myoid cells disrupts undifferentiated spermatogonial cell development. Proc. Natl. Acad. Sci. USA *113*, 1829–1834.

Cook, M.S., Munger, S.C., Nadeau, J.H., and Capel, B. (2011). Regulation of male germ cell cycle arrest and differentiation by DND1 is modulated by genetic background. Development *138*, 23–32.

Cool, J., DeFalco, T., and Capel, B. (2012). Testis formation in the fetal mouse: dynamic and complex de novo tubulogenesis. Wiley Interdiscip. Rev. Dev. Biol. *1*, 847–859.

Costoya, J.A., Hobbs, R.M., Barna, M., Cattoretti, G., Manova, K., Sukhwani, M., Orwig, K.E., Wolgemuth, D.J., and Pandolfi, P.P. (2004). Essential role of Plzf in maintenance of spermatogonial stem cells. Nat. Genet. *36*, 653–659.

De Gendt, K., Swinnen, J.V., Saunders, P.T., Schoonjans, L., Dewerchin, M., Devos, A., Tan, K., Atanassova, N., Claessens, F., Lécureuil, C., et al. (2004). A Sertoli cell-selective knockout of the androgen receptor causes spermatogenic arrest in meiosis. Proc. Natl. Acad. Sci. USA *101*, 1327–1332.

França, L.R., Hess, R.A., Dufour, J.M., Hofmann, M.C., and Griswold, M.D. (2016). The Sertoli cell: one hundred fifty years of beauty and plasticity. Andrology *4*, 189–212.

Gao, Y., and Cheng, C.Y. (2016). Does cell polarity matter during spermatogenesis? Spermatogenesis *6*, e1218408.

Gao, Y., Lui, W.Y., Lee, W.M., and Cheng, C.Y. (2016a). Polarity protein Crumbs homolog-3 (CRB3) regulates ectoplasmic specialization dynamics through its action on F-actin organization in Sertoli cells. Sci. Rep. *6*, 28589.

Gao, Y., Xiao, X., Lui, W.Y., Lee, W.M., Mruk, D., and Cheng, C.Y. (2016b). Cell polarity proteins and spermatogenesis. Semin. Cell Dev. Biol. *59*, 62–70.

Glogauer, M., Marchal, C.C., Zhu, F., Worku, A., Clausen, B.E., Foerster, I., Marks, P., Downey, G.P., Dinauer, M., and Kwiatkowski, D.J. (2003). Rac1 deletion in mouse neutrophils has selective effects on neutrophil functions. J. Immunol. *170*, 5652–5657.

Guo, L., Moon, C., Niehaus, K., Zheng, Y., and Ratner, N. (2012). Rac1 controls Schwann cell myelination through cAMP and NF2/merlin. J. Neurosci. *32*, 17251–17261.

Hedger, M.P., and Winnall, W.R. (2012). Regulation of activin and inhibin in the adult testis and the evidence for functional roles in spermatogenesis and immunoregulation. Mol. Cell. Endocrinol. *359*, 30–42.

Heinrich, A., and DeFalco, T. (2019). Essential roles of interstitial cells in testicular development and function. Andrology *24*. https://doi.org/10.1111/andr.12703.

Hess, R.A., Cooke, P.S., Bunick, D., and Kirby, J.D. (1993). Adult testicular enlargement induced by neonatal hypothyroidism is accompanied by increased Sertoli and germ cell numbers. Endocrinology *132*, 2607–2613.

Hill, C.M., Anway, M.D., Zirkin, B.R., and Brown, T.R. (2004). Intratesticular androgen levels, androgen receptor localization, and androgen receptor expression in adult rat Sertoli cells. Biol. Reprod. *71*, 1348–1358.

Inselman, A., Eaker, S., and Handel, M.A. (2003). Temporal expression of cell cycle-related proteins during spermatogenesis: establishing a timeline for onset of the meiotic divisions. Cytogenet. Genome Res. *103*, 277–284.

Jaegle, M., Ghazvini, M., Mandemakers, W., Piirsoo, M., Driegen, S., Levavasseur, F., Raghoenath, S., Grosveld, F., and Meijer, D. (2003). The POU proteins Brn-2 and Oct-6 share important functions in Schwann cell development. Genes Dev. *17*, 1380–1391.

Jameson, S.A., Natarajan, A., Cool, J., DeFalco, T., Maatouk, D.M., Mork, L., Munger, S.C., and Capel, B. (2012). Temporal transcriptional profiling of somatic and germ cells reveals biased lineage priming of sexual fate in the fetal mouse gonad. PLoS Genet. *8*, e1002575.

Joyce, K.L., Porcelli, J., and Cooke, P.S. (1993). Neonatal goitrogen treatment increases adult testis size and sperm production in the mouse. J. Androl. *14*, 448–455.

Kanatsu-Shinohara, M., and Shinohara, T. (2013). Spermatogonial stem cell self-renewal and development. Annu. Rev. Cell Dev. Biol. *29*, 163–187.

Kluin, P.M., Kramer, M.F., and de Rooij, D.G. (1984). Proliferation of spermatogonia and Sertoli cells in maturing mice. Anat. Embryol. (Berl.) *169*, 73–78.

Kumar, T.R., Wang, Y., Lu, N., and Matzuk, M.M. (1997). Follicle stimulating hormone is required for ovarian follicle maturation but not male fertility. Nat. Genet. *15*, 201–204.

Lindeboom, F., Gillemans, N., Karis, A., Jaegle, M., Meijer, D., Grosveld, F., and Philipsen, S. (2003). A tissue-specific knockout reveals that Gata1 is not essential for Sertoli cell function in the mouse. Nucleic Acids Res. *31*, 5405–5412.

Meachem, S.J., Nieschlag, E., and Simoni, M. (2001). Inhibin B in male reproduction: pathophysiology and clinical relevance. Eur. J. Endocrinol. *145*, 561–571.

Meinhardt, A., and Hedger, M.P. (2011). Immunological, paracrine and endocrine aspects of testicular immune privilege. Mol. Cell. Endocrinol. *335*, 60–68.

Meng, X., Lindahl, M., Hyvönen, M.E., Parvinen, M., de Rooij, D.G., Hess, M.W., Raatikainen-Ahokas, A., Sainio, K., Rauvala, H., Lakso, M., et al. (2000). Regulation of cell fate decision of undifferentiated spermatogonia by GDNF. Science *287*, 1489–1493.

Michaelson, D., Abidi, W., Guardavaccaro, D., Zhou, M., Ahearn, I., Pagano, M., and Philips, M.R. (2008). Rac1 accumulates in the nucleus during the G2 phase of the cell cycle and promotes cell division. J. Cell Biol. *181*, 485–496.

Ngok, S.P., Lin, W.H., and Anastasiadis, P.Z. (2014). Establishment of epithelial polarity–GEF who's minding the GAP? J. Cell Sci. *127*, 3205–3215.

Oatley, J.M., and Brinster, R.L. (2012). The germline stem cell niche unit in mammalian testes. Physiol. Rev. *92*, 577–595.

Oatley, M.J., Racicot, K.E., and Oatley, J.M. (2011). Sertoli cells dictate spermatogonial stem cell niches in the mouse testis. Biol. Reprod. *84*, 639–645.

Olson, M.F., Ashworth, A., and Hall, A. (1995). An essential role for Rho, Rac, and Cdc42 GTPases in cell cycle progression through G1. Science *269*, 1270–1272.

Orth, J.M. (1982). Proliferation of Sertoli cells in fetal and postnatal rats: a quantitative autoradiographic study. Anat. Rec. *203*, 485–492.

Potter, S.J., and DeFalco, T. (2017). Role of the testis interstitial compartment in spermatogonial stem cell function. Reproduction *153*, R151–R162.

Russell, L.D., Goh, J.C., Rashed, R.M., and Vogl, A.W. (1988). The consequences of actin disruption at Sertoli ectoplasmic specialization sites facing spermatids after in vivo exposure of rat testis to cytochalasin D. Biol. Reprod. *39*, 105–118.

Schneider, C.A., Rasband, W.S., and Eliceiri, K.W. (2012). NIH Image to ImageJ: 25 years of image analysis. Nat. Methods *9*, 671–675.

Sharpe, R.M., McKinnell, C., Kivlin, C., and Fisher, J.S. (2003). Proliferation and functional maturation of Sertoli cells, and their relevance to disorders of testis function in adulthood. Reproduction *125*, 769–784.

Stévant, I., Neirijnck, Y., Borel, C., Escoffier, J., Smith, L.B., Antonarakis, S.E., Dermitzakis, E.T., and Nef, S. (2018). Deciphering Cell Lineage Specification during Male Sex Determination with Single-Cell RNA Sequencing. Cell Rep. *22*, 1589–1599.

Stevens, L.C. (1973). A new inbred subline of mice (129-terSv) with a high incidence of spontaneous congenital testicular teratomas. J. Natl. Cancer Inst. *50*, 235–242.

Su, W., Wong, E.W., Mruk, D.D., and Cheng, C.Y. (2012). The Scribble/Lgl/Dlg polarity protein complex is a regulator of blood-testis barrier dynamics and spermatid polarity during spermatogenesis. Endocrinology *153*, 6041–6053.

Takashima, S., Kanatsu-Shinohara, M., Tanaka, T., Takehashi, M., Morimoto, H., and Shinohara, T. (2011). Rac mediates mouse spermatogonial stem cell homing to germline niches by regulating transmigration through the blood-testis barrier. Cell Stem Cell *9*, 463–475.

Vassalli, A., Matzuk, M.M., Gardner, H.A., Lee, K.F., and Jaenisch, R. (1994). Activin/inhibin beta B subunit gene disruption leads to defects in eyelid development and female reproduction. Genes Dev. *8*, 414–427.

Wong, E.W., Mruk, D.D., Lee, W.M., and Cheng, C.Y. (2008). Par3/Par6 polarity complex coordinates apical ectoplasmic specialization and blood-testis barrier restructuring during spermatogenesis. Proc. Natl. Acad. Sci. USA *105*, 9657–9662.

Wreford, N.G., Rajendra Kumar, T., Matzuk, M.M., and de Kretser, D.M. (2001). Analysis of the testicular phenotype of the follicle-stimulating hormone beta-subunit knockout and the activin type II receptor knockout mice by stereological analysis. Endocrinology *142*, 2916–2920.

Xiong, Z., Wang, C., Wang, Z., Dai, H., Song, Q., Zou, Z., Xiao, B., Zhao, A.Z., Bai, X., and Chen, Z. (2018). Raptor directs Sertoli cell cytoskeletal organization and polarity in the mouse testis. Biol. Reprod. *99*, 1289–1302.

Yomogida, K., Ohtani, H., Harigae, H., Ito, E., Nishimune, Y., Engel, J.D., and Yamamoto, M. (1994). Developmental stage- and spermatogenic cycle-specific expression of transcription factor GATA-1 in mouse Sertoli cells. Development *120*, 1759–1766.

Youngren, K.K., Coveney, D., Peng, X., Bhattacharya, C., Schmidt, L.S., Nickerson, M.L., Lamb, B.T., Deng, J.M., Behringer, R.R., Capel, B., et al. (2005). The Ter mutation in the dead end gene causes germ cell loss and testicular germ cell tumours. Nature *435*, 360–364.

Zhou, Q., Nie, R., Li, Y., Friel, P., Mitchell, D., Hess, R.A., Small, C., and Griswold, M.D. (2008). Expression of stimulated by retinoic acid gene 8 (Stra8) in spermatogenic cells induced by retinoic acid: an in vivo study in vitamin A-sufficient postnatal murine testes. Biol. Reprod. *79*, 35–42.

STAR★METHODS

KEY RESOURCES TABLE

REAGENT or RESOURCE	SOURCE	IDENTIFIER
Antibodies		
Rabbit polyclonal anti-ACTA2	Abcam	Cat#ab5694; RRID: AB_2223021
Rabbit polyclonal anti-AIF1 (IBA1)	Wako	Cat#019-19741; RRID: AB_839504
Goat polyclonal anti-AMH (MIS)	Santa Cruz Biotechnology	Cat#sc-6886; RRID: AB_649207
Rabbit polyclonal anti-AR	Santa Cruz Biotechnology	Cat#sc-816; RRID: AB_1563391
Rat monoclonal anti-CD4 (clone RM4-5)	BioLegend	Cat#100505; RRID: AB_312708
Rat monoclonal anti-CD45 (clone 30-F11)	BioLegend	Cat#103101; RRID: AB_312966
Goat polyclonal anti-KIT (C-KIT)	R&D Systems	Cat#AF1356; RRID: AB_354750
Rabbit polyclonal anti-cleaved Caspase 3 (Asp175)	Cell Signaling Technology	Cat#9661S; RRID: AB_2341188
Rabbit polyclonal anti-CLDN11	Thermo Fisher Scientific	Cat#36-4500; RRID: AB_2533259
Goat polyclonal anti-CTNNB1	Santa Cruz Biotechnology	Cat#sc-1496; RRID: AB_1563968
Goat polyclonal anti-CYP17A1	Santa Cruz Biotechnology	Cat# sc-46081; RRID: AB_2088659
Rabbit polyclonal anti-DDX4 (MVH)	Abcam	Cat#ab13840; RRID: AB_443012
Rat monoclonal anti-GATA1 (clone N6)	Santa Cruz Biotechnology	Cat#sc-265; RRID: AB_627663
Goat polyclonal anti-GATA4	Santa Cruz Biotechnology	Cat#sc-1237; RRID: AB_2108747
Rabbit polyclonal anti-GDNF	Santa Cruz Biotechnology	Cat#sc-328; RRID: AB_2247684
Goat polyclonal anti-GFRA1	Neuromics	Cat#GT15004; RRID: AB_2307379
Rabbit polyclonal anti-Histone H2A.X, phospho (Ser139)	Millipore	Cat#07-164; RRID: AB_310406
Guinea pig polyclonal anti-H1T	Mary Ann Handel (Inselman et al., 2003)	N/A
Goat polyclonal anti-ITGB1	Novus/R&D Systems	Cat#AF2405-SP; RRID: AB_416591
Rat monoclonal anti-MHC Class II (I-A/I-E) (clone M5/114.15.2)	eBioscience/Thermo Fisher Scientific	Cat#14-5321-81; RRID: AB_467560
Rabbit monoclonal anti-MKI67 (Ki67) (clone SP6)	GeneTex	Cat# NBP1-88861; RRID: AB_422351
Rabbit polyclonal anti-PARD3 (Par3)	Novus	Cat#NBP1-88861; RRID: AB_11056253
Goat polyclonal anti-PECAM1	R&D Systems	Cat#AF3628; RRID: AB_2161028
Rat monoclonal anti-PECAM1 (clone MEC13.3)	BD Biosciences	Cat#553370; RRID: AB_394816
Rabbit polyclonal anti-SCRIB	Santa Cruz Biotechnology	Cat#sc-28737; RRID: AB_2184807
Rabbit monoclonal anti-phospho-Scribble (Ser1220) (clone D8A2)	Cell Signaling Technology	Cat#12316; RRID: AB_2797883
Rabbit polyclonal anti-SOX9	Millipore	Cat#AB5535; RRID: AB_2239761
Rabbit polyclonal anti-STRA8	Abcam	Cat#ab49602; RRID: AB_945678
Rat monoclonal anti-TRA98 (clone TRA98)	Abcam	Cat#ab82527; RRID: AB_1659152
Mouse monoclonal anti-TUBB3 (clone TUJ1)	BioLegend	Cat#801201; RRID: AB_2313773
Chicken polyclonal anti-Vimentin	BioLegend	Cat#919101; RRID: AB_2565208
Rat monoclonal anti-Vimentin (clone W16220A)	BioLegend	Cat#699301; RRID: AB_2716136
Mouse monoclonal anti-ZBTB16 (PLZF) (clone 2A9)	Millipore	Cat#OP128-100UG; RRID: AB_213280
Alexa Fluor 647-AffiniPure Donkey Anti-Rat IgG (H+L)	Jackson Immunoresearch	Cat#712-605-153; RRID:AB_2340694
Alexa Fluor 647 Donkey anti-Goat IgG (H+L)	Thermo Fisher Scientific	Cat#A-21447; RRID:AB_2535864
Alexa Fluor 647 Donkey anti-Rabbit IgG (H+L)	Thermo Fisher Scientific	Cat#A-31573, RRID:AB_2536183
Alexa Fluor 647 Goat anti-Mouse IgG2a	Thermo Fisher Scientific	Cat#A-21241, RRID:AB_2535810
Cy3 AffiniPure Donkey Anti-Rat IgG (H+L)	Jackson Immunoresearch	Cat#712-165-153, RRID:AB_2340667

(*Continued on next page*)

Continued		
REAGENT or RESOURCE	SOURCE	IDENTIFIER
Alexa Fluor 555 Donkey anti-Goat IgG (H+L)	Thermo Fisher Scientific	Cat#A-21432, RRID:AB_2535853
Alexa Fluor 555 Donkey anti-Rabbit IgG (H+L)	Thermo Fisher Scientific	Cat#A-31572, RRID:AB_162543
Alexa Fluor 555 Goat anti-Mouse IgG2a	Thermo Fisher Scientific	Cat#A-21137, RRID:AB_2535776
Alexa Fluor 488 Donkey anti-Rat IgG (H+L)	Thermo Fisher Scientific	Cat#A-21208, RRID:AB_141709
Alexa Fluor Plus 488 Donkey anti-Rabbit IgG (H+L)	Thermo Fisher Scientific	Cat#A32790, RRID:AB_2762833
Alexa Fluor 488 AffiniPure Donkey Anti-Chicken IgY (IgG) (H+L)	Jackson Immunoresearch	Cat#703-545-155, RRID:AB_2340375
Chemicals, Peptides, and Recombinant Proteins		
Alexa Fluor 647 Phalloidin	Thermo Fisher Scientific	Cat#A22287; RRID: AB_2620155
Rhodamine Phalloidin	Thermo Fisher Scientific	Cat#R415; RRID: AB_2572408
Hoechst 33342, Trihydrochloride, Trihydrate	Thermo Fisher Scientific	Cat#H1399
Streptavidin, Alexa Fluor 555 Conjugate	Thermo Fisher Scientific	Cat#S21381; RRID: AB_2307336
EZ-Link Sulfo-NHS-LC-Biotin, No-Weigh Format	Thermo Fisher Scientific	Cat#A39257
Experimental Models: Organisms/Strains		
Mouse: Dhh-Cre: Tg(Dhh-cre)1Mejr	Dies Meijr; (Jaegle et al., 2003; Lindeboom et al., 2003)	RRID: IMSR_JAX:012929
Mouse: Rac1$^{flox/flox}$: Rac1^{tm1Djk}/J	Yi Zheng; (Glogauer et al., 2003)	RRID: IMSR_JAX:005550
Mouse: CD-1 IGS Mouse: Crl:CD1(ICR)	Charles River	Cat#CRL:022; RRID: IMSR_CRL:022
Mouse: *Kit^{W}/Kit^{W-v}*: WBB6F1/J-Kit^{W}/Kit^{W-v}/J	The Jackson Laboratory	JAX: 100410; RRID: IMSR_JAX:100410
Mouse: *Dnd1^{Ter}*: *Dnd1^{Ter}*	Blanche Capel; (Stevens, 1973; Youngren et al., 2005)	MGI:2158668; RRID: MGI:3690452
Mouse: Rosa-tdTomato: B6.Cg-Gt(ROSA)26Sor$^{tm14(CAG-tdTomato)Hze}$/J	The Jackson Laboratory	JAX: 007914; RRID: IMSR_JAX:007914
Oligonucleotides		
Primers for quantitative real-time PCR (qPCR), see Table S1.	This paper	N/A
Software and Algorithms		
ImageJ	Schneider et al., 2012	https://imagej.nih.gov/ij/

LEAD CONTACT AND MATERIALS AVAILABILITY

Further information and requests for resources and reagents should be directed to and will be fulfilled by the Lead Contact, Tony DeFalco (tony.defalco@cchmc.org).

Key resources including details of key reagents are available in the Key Resources Table. This study did not generate any new unique reagents.

EXPERIMENTAL MODEL AND SUBJECT DETAILS

Mice

All mice used in these experiments were housed in the Cincinnati Children's Hospital Medical Center's animal care facility, in compliance with institutional and National Institutes of Health guidelines. All experimental protocols were approved by the Institutional Animal Care and Use Committee (IACUC) of Cincinnati Children's Hospital Medical Center. Animals were housed in a 12-hour light/12-hour dark cycle and had access to autoclaved rodent Lab Diet 5010 (Purina, St. Louis, MO, USA) and ultraviolet light-sterilized RO/DI constant circulation water *ad libitum*. *Dhh*-Cre (Tg(Dhh-cre)1Mejr) (Jaegle et al., 2003; Lindeboom et al., 2003) (obtained from Dies Meijer, University of Edinburgh) and *Rac1^{flox}* (*Rac1^{tm1Djk}*) (Glogauer et al., 2003) (obtained from Yi Zheng, Cincinnati Children's Hospital Medical Center) alleles were maintained on a C57BL/6J background. *Dhh*-Cre hemizygous;*Rac1$^{flox/+}$* heterozygous males were crossed to homozygous *Rac1$^{flox/flox}$* females and their offspring were genotyped and used for analysis. In this study, only male (XY) animals were used due to our focus on testis development. *Dhh*-Cre;*Rac1$^{flox/flox}$* conditional knockout mice begin to exhibit partial hind limb paralysis around 3 weeks but can live a normal lifespan if continuously provided with food on the floor of their cages after weaning (Guo et al., 2012). *Dhh*-Cre was genotyped using primers (5′ to 3′) ACCCTGTTACGTATAGCCGA and CTCCGGTATTGAAACTCCAG, and confirmed via the presence of a 400bp band. The *Rac1^{flox}* allele was genotyped using primers TCCAATCTGTGCTGCCCATC, GATGCTTCTAGGGGTGAGCC, and CAGAGCTCGAATCCAGAAACTAGTA to determine

the presence of *Rac1*^{flox} (240bp), *Rac1*^{KO} (170bp), or WT (120bp) alleles. Both Cre-negative; *Rac1*$^{flox/flox}$ homozygous and Cre-positive; *Rac1*$^{flox/+}$ heterozygous littermates were used as controls. Adult *Kit*^{W}/*Kit*$^{W-v}$ compound heterozygous males (WBB6F1/J-*Kit*^{W}/*Kit*$^{W-v}$/J) were obtained from the Jackson Laboratory (stock #100410), on mixed background of WB/ReJ and C57BL/6J. *Dnd1*^{Ter} mice (Stevens, 1973; Youngren et al., 2005) were obtained from Blanche Capel (Duke University Medical Center); *Dnd1*^{Ter} mice were originally on a 129T2/SvEmsJ background, but were backcrossed to C57BL/6J for 3 generations to eliminate the occurrence of testicular teratomas while maintaining complete germ cell depletion (Cook et al., 2011). *Dnd1*$^{Ter/Ter}$ homozygous mice were obtained via intercross of *Dnd1*$^{Ter/+}$ heterozygous animals and were genotyped using a Custom TaqMan SNP Genotyping Assay (Applied Biosystems/Thermo Fisher #4332077). *Rosa*-tdTomato mice (B6.Cg-*Gt(ROSA)26Sor*$^{tm14(CAG-tdTomato)Hze}$/J) were obtained from the Jackson Laboratory (stock #007914) and were maintained on a C57BL/6J background. Outbred CD-1 mice (Charles River) were used for E13.5 wild-type analyses. For embryonic/fetal time points, timed matings were arranged, and noon on the day that vaginal plugs were detected was considered E0.5.

METHOD DETAILS

Immunofluorescence

Testes were dissected in PBS and fixed overnight in 4% paraformaldehyde (PFA) with 0.1% Triton X-100. To assist with fixation of adult testes, the capsule was superficially punctured 10-12 times with a 27-gauge needle before fixation; after overnight fixation, testes were cut in half transversely with a fresh razor blade the next morning and placed again in 4% PFA for 2 additional hours to continue fixing. After several washes in PBS + 0.1% Triton X-100 (PBTx), samples were processed through a sucrose:PBS gradient (10%, 15%, 20% sucrose) before an overnight incubation in a 1:1 mixture of 20% sucrose and OCT medium (Sakura) rocking at 4°C. Samples were embedded in OCT medium at −80°C prior to cryosectioning. After cryosectioning at 16-20 μM (depending on age of sample), samples were washed several times in PBTx, then incubated in blocking solution (PBTx + 10% fetal bovine serum [FBS] + 10% bovine serum albumin [BSA]) for 1 hour at room temperature. Primary antibodies were diluted in blocking solution and applied to samples overnight at 4°C. Primary antibodies used were: rabbit anti-ACTA2 (SMA) (Abcam, 1:500); rabbit anti-AIF1 (IBA1) (Wako, 1:1,000); goat anti-AMH (MIS) (Santa Cruz, 1:500); rabbit anti-AR (Santa Cruz, 1:300); rat anti-CD4 (clone RM4-5) (BioLegend, 1:300); rat anti-CD45 (clone 30-F11) (BioLegend, 1:300); goat anti-KIT (C-KIT) (R&D, 1:400); rabbit anti-cleaved Caspase 3 (Asp175) (Cell Signaling, 1:250); rabbit anti-CLDN11 (Thermo Fisher, 1:1,000); goat anti-CTNNB1 (Santa Cruz, 1:400); goat anti-CYP17A1 (Santa Cruz, 1:500); rabbit anti-DDX4 (MVH) (Abcam, 1:1,000); rat anti-GATA1 (clone N6) (Santa Cruz, 1:1,000); goat anti-GATA4 (Santa Cruz, 1:100); rabbit anti-GDNF (Santa Cruz, 1:500); goat anti-GFRA1 (Neuromics, 1:200); rabbit anti-Histone H2A.X, phospho (Ser139) (Millipore, 1:1,000); guinea pig anti-H1T (Mary Ann Handel (Inselman et al., 2003), 1:2,000); goat anti-ITGB1 (Novus/R&D, 1:500); rat anti-MHC Class II (I-A/I-E) (clone M5/114.15.2) (eBioscience/Thermo Fisher, 1:500); rabbit anti-MKI67 (Ki67) (clone SP6) (GeneTex, 1:300); rabbit anti-PARD3 (Par3) (Novus, 1:100); goat anti-PECAM1 (R&D, 1:300); rat anti-PECAM1 (clone MEC13.3) (BD Biosciences, 1:250); rabbit anti-SCRIB (Santa Cruz, 1:300); rabbit anti-phospho-Scribble (Ser1220) (clone D8A2) (Cell Signaling, 1:500); rabbit anti-SOX9 (Millipore, 1:4,000); rabbit anti-STRA8 (Abcam, 1:3,000); rat anti-TRA98 (clone TRA98) (Abcam, 1:1,000); mouse anti-TUBB3 (clone TUJ1) (BioLegend, 1:1,000); chicken anti-Vimentin (BioLegend, 1:1,000); rat anti-Vimentin (clone W16220A) (BioLegend, 1:1,000); and mouse anti-ZBTB16 (PLZF) (clone 2A9) (Millipore, 1:250). After several washes in PBTx, fluorescent secondary antibodies (Alexa 488-, Alexa-555-, Alexa-647-, or Cy3-conjugated; from Molecular Probes/Thermo Fisher or Jackson Immunoresearch, all at 1:500 dilution) and nuclear dye (2 μg/ml Hoechst 33342, #H1399, Molecular Probes/Life Technologies/Thermo Fisher) were diluted in blocking solution and applied for 1 hour at room temperature. After several washes in PBTx, samples were mounted on slides in Fluoromount-G (SouthernBiotech). Samples were imaged either on a Nikon Eclipse TE2000 microscope (Nikon, Tokyo, Japan) with an Opti-Grid structured illumination imaging system using Volocity software (PerkinElmer, Waltham, MA, USA) or on a Nikon A1 Inverted Confocal Microscope (Nikon, Tokyo, Japan). Unless otherwise noted, at least 3 sections from at least n = 3 independent, individual animals (i.e., n = 3 independent biological replicates) were examined for each time point (i.e., fetal stage or age) and/or experimental condition.

Cell counts and tubule area quantification

Fiji/ImageJ (NIH) was used to analyze images for both cell counts and tubule area quantifications. For cell counts, the Cell Counter plug-in was used to manually count positive cells per tubule. For measuring tubule cross-sectional areas, the perimeters of individual tubules were outlined using the Polygon Selection tool, and the area in pixels was calculated with the Measure function. Pixel area was then converted to square microns based on the pixel dimensions of each image. For cell counts and tubule quantifications, measurements were taken from at least 3 different cryosections (cross-sections) per testis, from n = 3 testes, each from an independent male. Sample sizes used for each experiment are noted in the corresponding figure legend, but generally were between 10-50 tubules analyzed per testis (30-150 total tubules). Graph results are shown as mean ± SD. Statistical analyses were performed using a two-tailed Student t test, and a *P value* of $p < 0.05$ was considered statistically significant.

RNA extraction, cDNA synthesis, and quantitative real-time PCR

Total RNA was extracted and processed for quantitative real-time PCR. Tissue was homogenized by vortexing in 800 μL TRIzol reagent (Invitrogen/Thermo Fisher). RNA extraction was then performed using a TRIzol/isopropanol precipitation method. Briefly,

200 μL of chloroform was added to the Trizol/tissue mixture, shaken by hand, incubated at room temperature for 3 minutes, and centrifuged at 12,000 x *g* for 10 minutes at 4°C. The upper aqueous layer was carefully recovered and added to 400 μL isopropanol, which was rocked at room temperature for 10 minutes. After centrifugation at 12,000 x *g* for 10 minutes at 4°C, supernatant was removed and the pellet was washed with 500 μL of ethanol. After another centrifugation (with same parameters), the RNA pellet was briefly air-dried and diluted in nuclease-free water. RNA quality was assessed by spectrophotometric analysis via absorbance at 260 and 280 nm, in which only RNA samples with a 260/280 ratio greater than or equal to 1.6 was used for quantitative real-time PCR analysis (sample ratios were usually between 1.7-2.0). An iScript cDNA synthesis kit (BioRad) was used on 500ng of RNA for cDNA synthesis, as per manufacturer's instructions. Quantitative real-time PCR was performed using the Fast SYBR Green Master Mix (Applied Biosystems/Thermo Fisher) on the StepOnePlus Real-Time PCR system (Applied Biosystems/Thermo Fisher). The following parameters were used: 95°C for 20 s, followed by 40 cycles of 95°C for 3 s and 60°C for 30 s, followed by a melt curve run. Primer specificity for a single amplicon was verified by melt curve analysis. *Gapdh* was used as an internal normalization control. Fold change in mRNA levels was calculated relative to controls using a ΔΔCt method. A two-tailed Student t test was performed to calculate *P value*s, in which $p < 0.05$ was considered statistically significant. Sequences of primers used in this study are listed in Table S1.

Hormone measurements

Testosterone (T), luteinizing hormone (LH), follicle stimulating hormone (FSH), and inhibin B measurements were performed by the Ligand Assay and Analysis Core of the University of Virginia Center for Research in Reproduction. For testis homogenate measurements, whole adult testes were mechanically lysed with mortar and pestle in 500 uL PBS, sonicated for 60 s to ensure cell disruption, and centrifuged at 12,000 x *g* at 4°C for 10 minutes to remove cellular debris. Supernatant was collected and stored at −80°C until analyzed. For serum measurements, whole blood was collected from the posterior vena cava, allowed to clot at room temperature for 90 minutes, after which a sterile pipet tip was run along tube's interior wall to disrupt adhesion of the clot to the tube wall. Samples were centrifuged at 2,000 x *g* for 15 minutes at room temperature. After centrifugation, serum was removed and stored at −80°C until analyzed.

Biotin tracer injections

One-month-old (P30) male mice were anesthetized via inhaled isoflurane before a small incision was made in the lower abdomen, exposing the abdominal cavity. Using forceps to grip the epididymal fat pads, the testis was then gently pulled out of the abdomen. Twenty microliters of either 1mM $CaCl_2$ (in PBS) alone for one testis, or 1mM $CaCl_2$ with 10 mg/mL Biotin (EZ-Link Sulfo-NHS-LC-Biotin, No-Weigh Format; Thermo Fisher #A39257) for the contralateral experimental testis was injected. Testes were then replaced into the abdominal cavity and the incision closed. Mice were kept under anesthesia via isoflurane for an additional 30 minutes before being euthanized by cervical dislocation. Testes were harvested, fixed, and prepared for cryosectioning and immunofluorescence as described above. To detect biotin binding in testicular cryosections, Alexa Fluor-555-conjugated streptavidin (Thermo Fisher #S21381, 2 μg/ml) was used for 1 hour at room temperature, along with Hoechst 33342 dye to stain nuclei.

QUANTIFICATION AND STATISTICAL ANALYSIS

Statistical details of experiments, such as the exact value of n, what n represents, precision measures (mean ± SD), and statistical significance can be found in the Figure Legends.

Statistical analysis was performed using Excel (Microsoft). Statistical significance was defined as $p < 0.05$. For cell counts and tubule area quantifications, a two-tailed Student t test was performed on control versus cKO samples. For quantitative real-time PCR, a two-tailed Student t test was performed based on delta Ct values (normalized to *Gapdh*) for each gene for control versus cKO samples.

DATA AND CODE AVAILABILITY

This study did not generate or analyze any unique datasets or code.

Cell Reports, Volume *31*

Supplemental Information

Distinct Roles for *Rac1* in Sertoli Cell Function during Testicular Development and Spermatogenesis

Anna Heinrich, Sarah J. Potter, Li Guo, Nancy Ratner, and Tony DeFalco

Figure S1

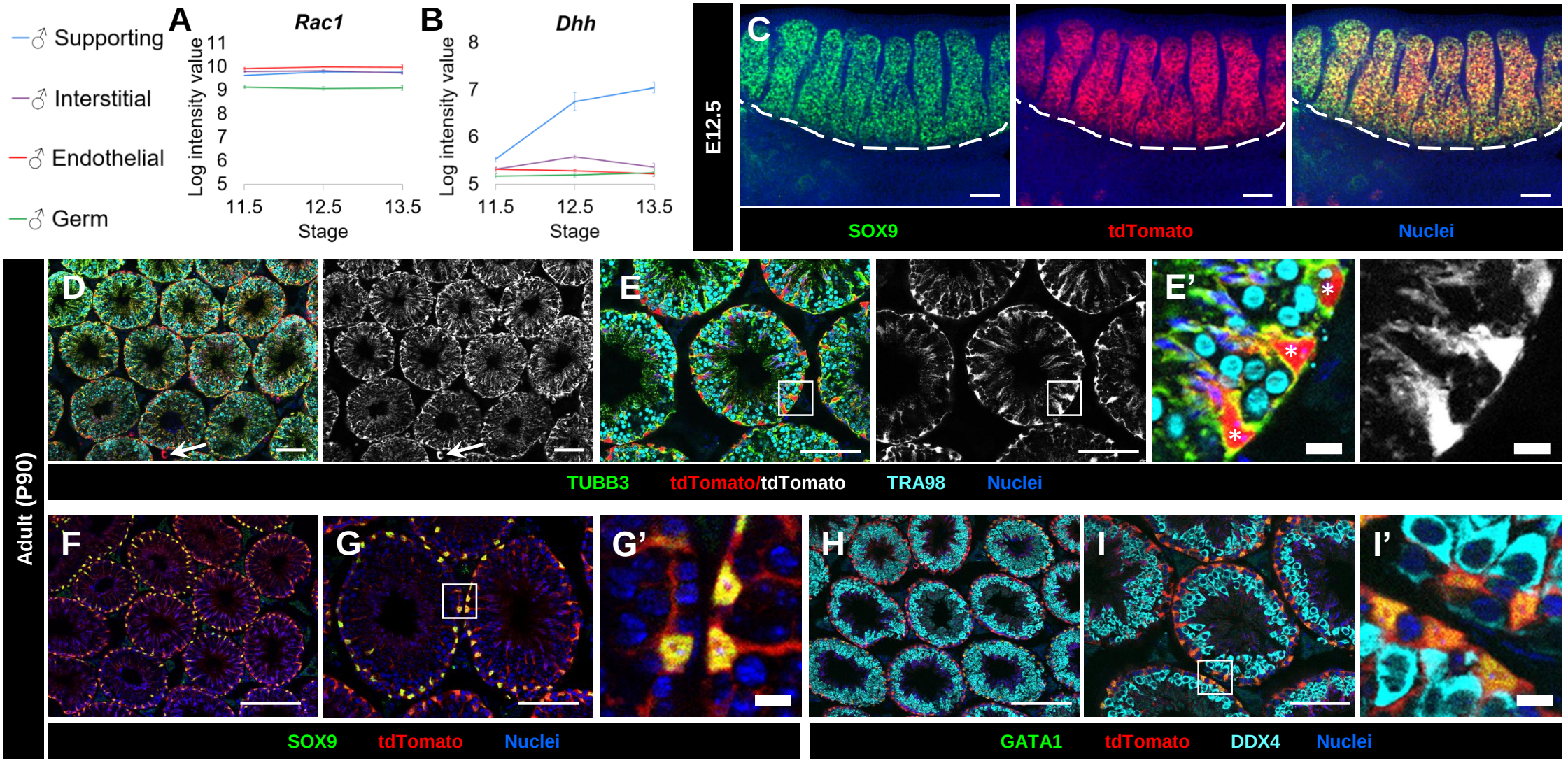
♂ Supporting
♂ Interstitial
♂ Endothelial
♂ Germ
A
Rac1
Log intensity value
11
10
9
8
7
6
5
11.5
12.5
13.5
Stage
B
Dhh
Log intensity value
8
7
6
5
11.5
12.5
13.5
Stage
E12.5
C
SOX9
tdTomato
Nuclei
Adult (P90)
D
E
E'
TUBB3
tdTomato/tdTomato
TRA98
Nuclei
F
G
G'
SOX9
tdTomato
Nuclei
H
I
I'
GATA1
tdTomato
DDX4
Nuclei

Figure S1. *Dhh*-Cre is highly efficient and specific for targeting Sertoli cells, Related to Figure 1.

(A,B) Plots showing gene expression levels of *Rac1* and *Dhh* expression, which were generated from fetal gonad cell-type-specific microarray data (Jameson et al., 2012), where cell lineages (supporting Sertoli cells, interstitial cells, endothelial cells, and germ cells) were independently plotted in different colors. Graph contains data for E11.5, E12.5, and E13.5 XY gonads for each cell type. In general, expression values below 6 are considered background expression levels. *Rac1* is expressed at high levels in all cell types, while *Dhh* becomes highly specific to Sertoli cells early in testicular development. (C-I) Immunofluorescence images of E12.5 (C) and adult P90 (D-I) *Dhh*-Cre; *Rosa*-tdTomato testes. E', G' and I' are higher-magnification images of the boxed regions in E, G, and I. Dashed line in C indicates gonad-mesonephros border. (C) tdTomato specifically co-localizes with Sertoli marker SOX9 in E12.5 fetal testes. (D-I) Lineage tracing of *Dhh*-Cre activity into adulthood reveals highly efficient tdTomato labeling in TUBB3/SOX9/GATA1-positive Sertoli cells, with no labeling in TRA98/DDX4-positive germ cells. We occasionally observed mosaic Cre activity in vasculature-associated cells (arrow in D), as has been previously reported in the testis (Lindeboom et al., 2003). Thin scale bar, 100 μm; thick scale bar 10 μm.

Figure S2

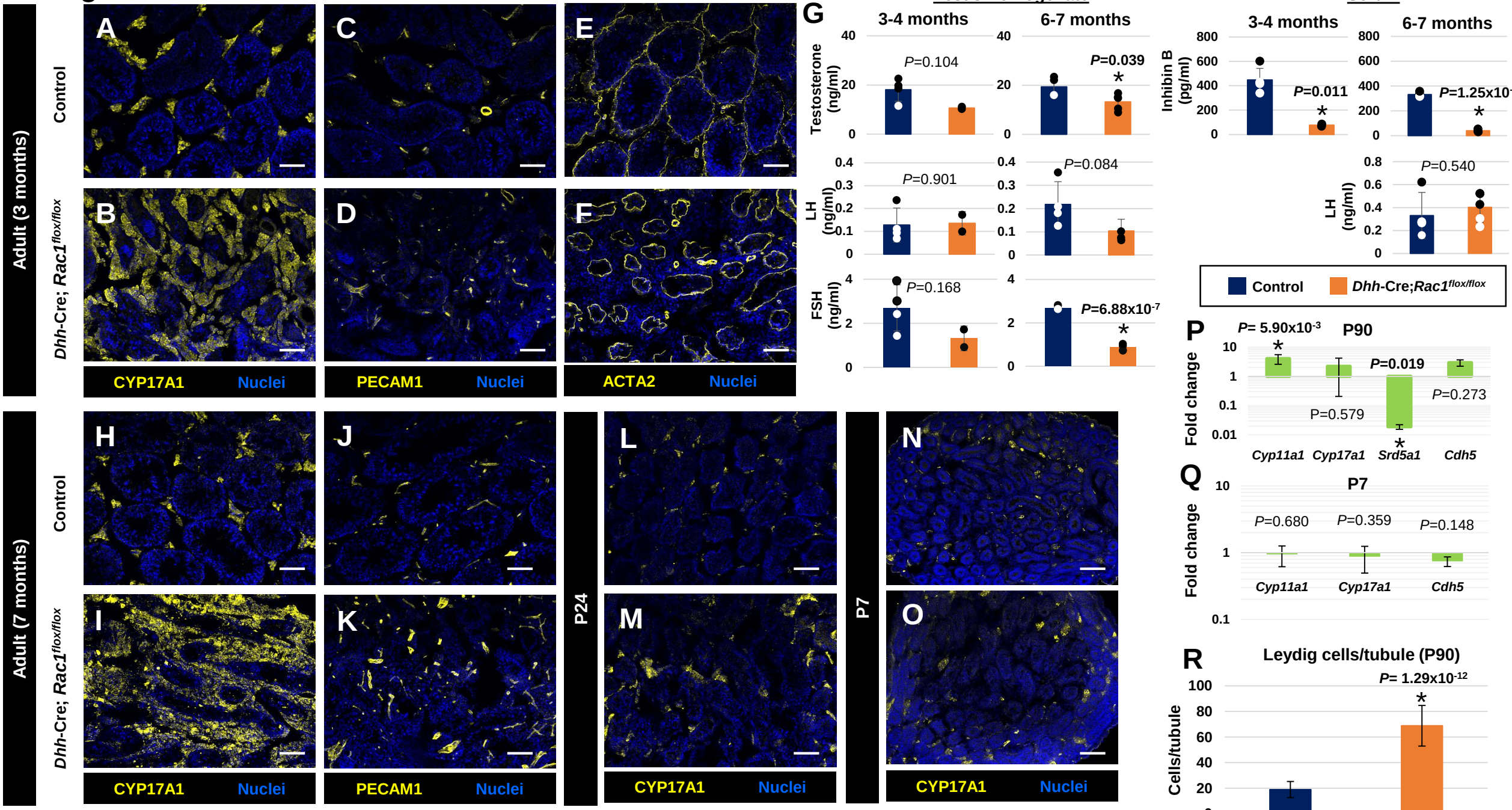
Adult (3 months)
Control
Dhh-Cre; Rac1flox/flox
A
B
C
D
E
F
CYP17A1
Nuclei
PECAM1
Nuclei
ACTA2
Nuclei
G
Testis Homogenate
3-4 months
6-7 months
Testosterone (ng/ml)
P=0.104
P=0.039
LH (ng/ml)
P=0.901
P=0.084
FSH (ng/ml)
P=0.168
P=6.88x10-7
Serum
3-4 months
6-7 months
Inhibin B (pg/ml)
P=0.011
P=1.25x10-8
LH (ng/ml)
P=0.540
Control
Dhh-Cre;Rac1flox/flox
Adult (7 months)
Control
Dhh-Cre; Rac1flox/flox
H
I
J
K
CYP17A1
Nuclei
PECAM1
Nuclei
P24
L
M
CYP17A1
Nuclei
P7
N
O
CYP17A1
Nuclei
P
P90
P= 5.90x10-3
P=0.579
P=0.019
P=0.273
Fold change
Cyp11a1
Cyp17a1
Srd5a1
Cdh5
Q
P7
P=0.680
P=0.359
P=0.148
Fold change
Cyp11a1
Cyp17a1
Cdh5
R
Leydig cells/tubule (P90)
P= 1.29x10-12
Cells/tubule

Figure S2. *Rac1* deletion in Sertoli cells has minimal effects on vascular and Leydig cell development, but disrupts some aspects of hormone production, Related to Figure 1.

(A-F) Immunofluorescence images of 3-month-old (P90) adult control *Dhh*-Cre;*Rac1*$^{flox/+}$ (A,C,E) and *Dhh*-Cre;*Rac1*$^{flox/flox}$ cKO (B,D,F) testes, showing normal expression of CYP17A1 (Leydig cells), PECAM1 (endothelial cells), and ACTA2 (also known as SMA; marker for peritubular myoid cells and vascular smooth muscle). (G) Graphs showing levels of various hormones in testis homogenate or blood serum from control versus cKO adult males. Each dot in the graphs represents an independent testis or serum sample. Left side shows testicular testosterone (T), luteinizing hormone (LH), and follicle-stimulating hormone (FSH) in 3-4 month old (n=2-4) or 6-7 month old (n=2-4) males, with significantly decreased levels of T and FSH only occurring at 6-7 months old. Right side shows significantly decreased levels of serum Inhibin B in both 3-4 month old (n=2-4) and 6-7 month old (n=2-4) males, but normal levels of serum LH in 6-7 month old (n=2-4) males. Data are shown as mean ± SD. *P* values were calculated using a two-tailed Student t-test. (H-K) Immunofluorescence images of 7-month-old adult control *Dhh*-Cre;*Rac1*$^{flox/+}$ (H,J) and *Dhh*-Cre;*Rac1*$^{flox/flox}$ cKO (I,K) testes, showing expression of CYP17A1 and PECAM1. (L,M) Immunofluorescence images of P24 juvenile control *Dhh*-Cre;*Rac1*$^{flox/+}$ (L) and *Dhh*-Cre;*Rac1*$^{flox/flox}$ cKO (M) testes, showing expression of CYP17A1. (N,O) Immunofluorescence images of P7 postnatal control *Rac1*$^{flox/flox}$ (N) and *Dhh*-Cre;*Rac1*$^{flox/flox}$ cKO (O) testes, showing expression of CYP17A1. (P,Q) Quantitative PCR analyses showing fold change of gene expression in controls versus cKO testes (see above for description of controls at each age) at P90 (P) and P7 (Q) for Leydig cell genes *Cyp11a1* (n=5 for P7; n=4 for P90), *Cyp17a1* (n=5 for P7; n=5 for P90), and *Srd5a1* (n=3 for P90) and vascular endothelial *Cdh5* (n=5 for P7; n=3 for P90). (R) Graph showing average number of CYP17A1+ Leydig cells per tubule in control versus cKO P90 testes (n=31, 37, and 30 tubules each from 3 independent control males and n=45, 101, and 65 tubules each from 3 independent cKO males). Data are shown as mean ± SD. *P* values were calculated using a two-tailed Student t-test. Scale bar is 100 μm throughout all panels.

Figure S3

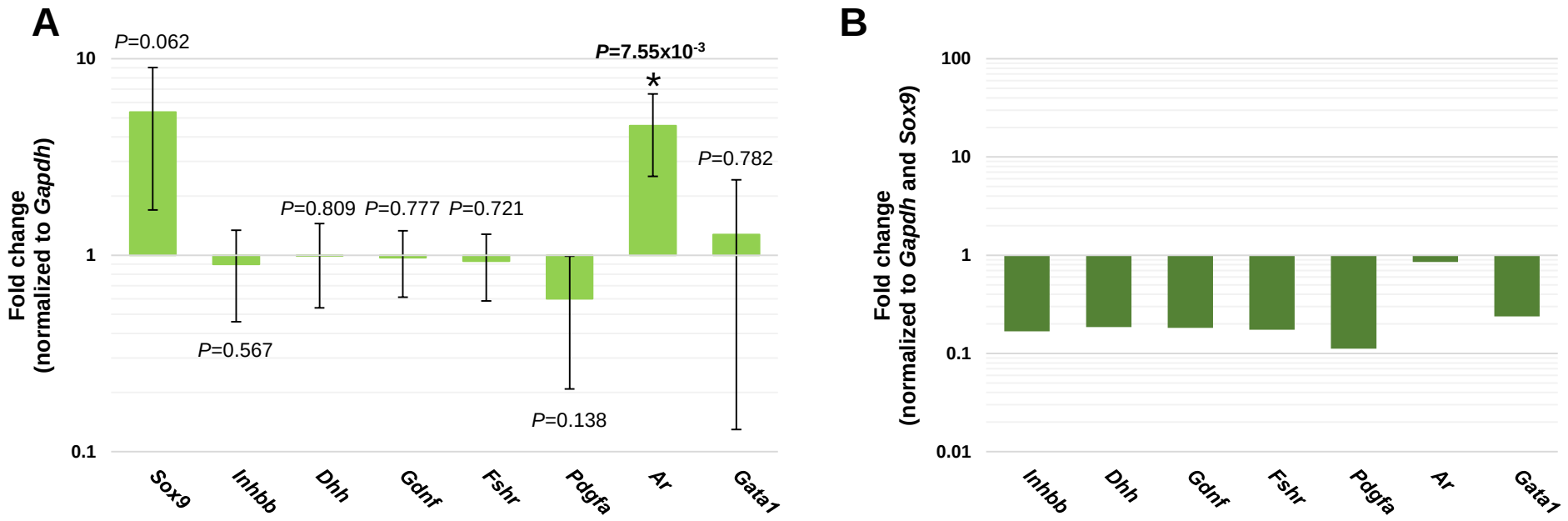
A
P=0.062
P=7.55x10-3
*
P=0.782
P=0.809
P=0.777
P=0.721
P=0.567
P=0.138
10
1
0.1
Fold change
(normalized to Gapdh)
Sox9
Inhbb
Dhh
Gdnf
Fshr
Pdgfa
Ar
Gata1
B
100
10
1
0.1
0.01
Fold change
(normalized to Gapdh and Sox9)
Inhbb
Dhh
Gdnf
Fshr
Pdgfa
Ar
Gata1

Figure S3. Expression of Sertoli-expressed differentiation markers and paracrine factors is reduced in adult cKO testes, Related to Figure 1.

(A) qPCR analyses of P90 *Dhh*-Cre;*Rac1*$^{flox/+}$ control versus *Dhh*-Cre;*Rac1*$^{flox/flox}$ cKO testes, focusing on genes expressed in Sertoli cells, encoding transcription factors (*Sox9*, *Gata1*), hormone receptors (*Fshr*, *Ar*), and paracrine secreted factors (*Inhbb*, *Dhh*, *Gdnf*, *Pdgfa*) (n=6 for *Sox9*; n=3 for *Inhbb*; n=3 for *Dhh*; n=3 for *Gdnf*; n=3 for *Fshr;* n=3 for *Pdgfa*; n=4 for *Ar*; n=3 for *Gata1*). (B) Same data as in A, except data was additionally normalized to *Sox9* (after normalization to *Gapdh*) by average fold change of cKO *Sox9* expression relative to controls. Data are shown as mean ± SD in A, and as mean in B. *P* values were calculated using a two-tailed Student t-test.

Figure S4

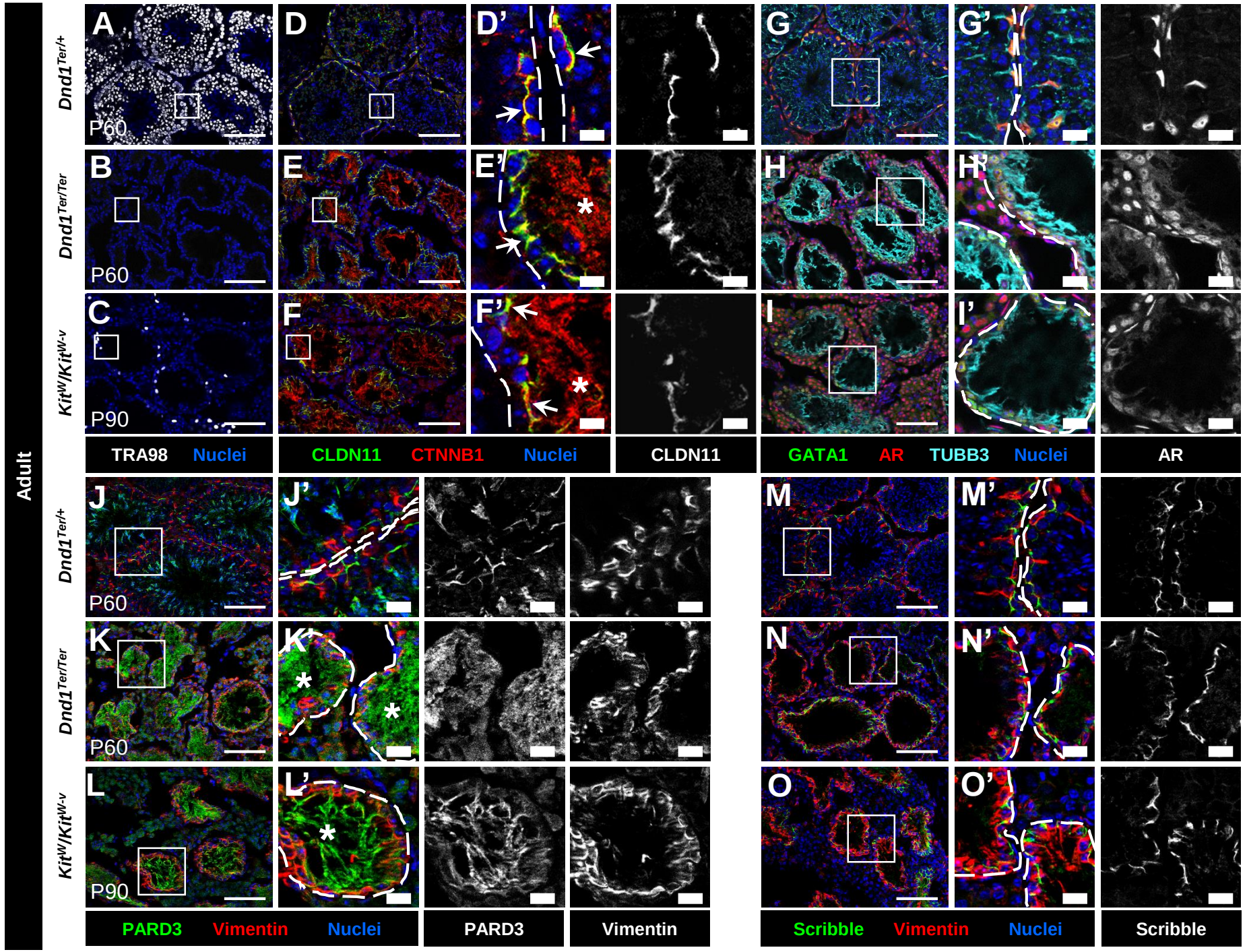
Adult
Dnd1Ter/+
Dnd1Ter/Ter
KitW/KitW-v
P60
P90
A
B
C
D
D'
E
E'
F
F'
G
G'
H
H'
I
I'
J
J'
K
K'
L
L'
M
M'
N
N'
O
O'
TRA98 Nuclei
CLDN11 CTNNB1 Nuclei
CLDN11
GATA1 AR TUBB3 Nuclei
AR
PARD3 Vimentin Nuclei
PARD3
Vimentin
Scribble Vimentin Nuclei
Scribble

Figure S4. Localization of apicobasal polarity markers and BTB proteins are mostly, but not completely, maintained in mouse models of germ cell deficiency, Related to Figure 4.

(A-O) Immunofluorescent images of P60 *Dnd1*$^{Ter/+}$ control (A,D,G,J,M), P60 *Dnd1*$^{Ter/Ter}$ mutant (B,E,H,K,N), and P90 *Kit*^{W}/*Kit*$^{W\text{-}v}$ compound heterozygous mutant (C,F,I,L,O) testes. D'-O' are higher-magnification images of the boxed regions in D-O. Dashed lines throughout indicate tubule boundaries. (A-C) TRA98 staining reveals extent of germ cell loss in *Ter* and *Kit* mutants. (D-F) CLDN11/CTNNB1 staining outlines normal BTB structure in all models (arrows); however, CTNNB1 expression is also expanded throughout Sertoli cells in germ-cell-deficient testes (asterisks in E' and F'). (G-I) AR nuclear localization is largely maintained in Sertoli cells in all models, although some weak cytoplasmic expression is observed in germ-cell-deficient testes. (J-L) While basal localization of Vimentin is maintained in all samples, PARD3 localization is perturbed in germ-cell-deficient testes (asterisks in K' and L'). (M-O) Scribble expression is maintained normally, i.e., along the BTB and in the basal compartment, in all testes. Thin scale bar, 100 μm; thick scale bar 10 μm.

Figure S5

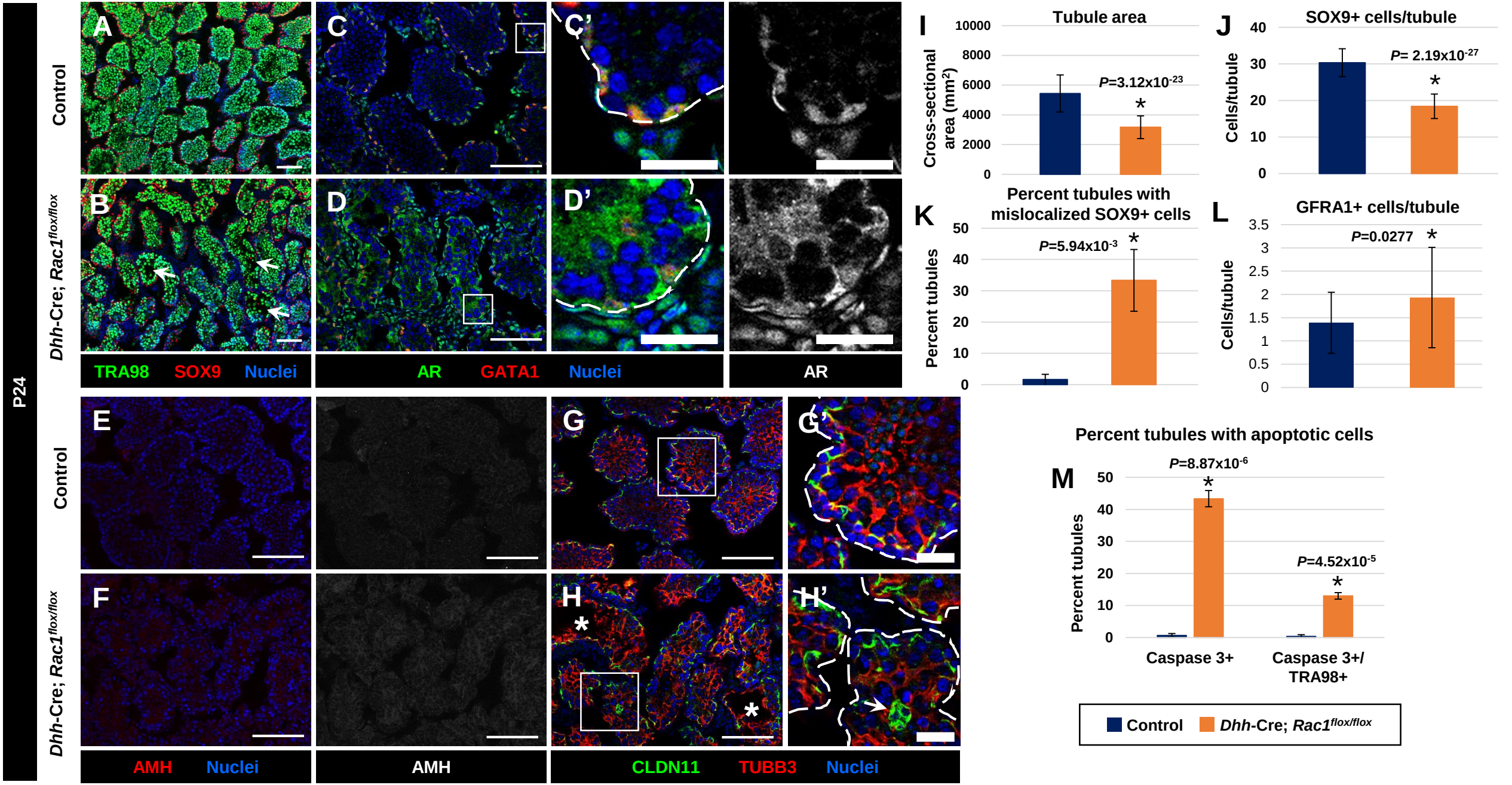
P24
Control
Dhh-Cre; Rac1flox/flox
A
B
C
C'
D
D'
TRA98 SOX9 Nuclei
AR GATA1 Nuclei
AR
E
F
G
G'
H
H'
AMH Nuclei
AMH
CLDN11 TUBB3 Nuclei
I
Tubule area
Cross-sectional area (mm2)
10000
8000
6000
4000
2000
0
P=3.12x10-23
J
SOX9+ cells/tubule
Cells/tubule
40
30
20
10
0
P= 2.19x10-27
K
Percent tubules with mislocalized SOX9+ cells
Percent tubules
50
40
30
20
10
0
P=5.94x10-3
L
GFRA1+ cells/tubule
Cells/tubule
3.5
3
2.5
2
1.5
1
0.5
0
P=0.0277
M
Percent tubules with apoptotic cells
Percent tubules
50
40
30
20
10
0
P=8.87x10-6
P=4.52x10-5
Caspase 3+
Caspase 3+/ TRA98+
Control
Dhh-Cre; Rac1flox/flox

Figure S5. Onset of testis dysgenesis is evident in juvenile (P24) *Rac1* cKO males, Related to Figure 6.

(A-H) Immunofluorescence images of P24 control *Dhh*-Cre;*Rac1*$^{flox/+}$ (A,C,E,G) and *Dhh*-Cre;*Rac1*$^{flox/flox}$ cKO (B,D,F,H) testes. C', D', G', and H' are higher-magnification images of the boxed regions in C, D, G, and H. Dashed lines throughout indicate tubule boundaries. (A,B) TRA98 staining reveals patchy germ cell loss in cKO tubules (arrows in B). (C,D) AR subcellular (nuclear) localization is disrupted in cKO tubules. (E,F) AMH expression is not substantially affected in cKO testes. (G,H) CLDN11 staining shows a grossly normal initial formation of the BTB; however, there are aberrant CLDN11 aggregates often seen in the middle of cKO tubules (arrow in H'). Vacuolization of Sertoli cells (TUBB3+) is often seen in cKO tubules (asterisks in H), likely due to germ cell loss. Thin scale bar, 100 μm; thick scale bar 25 μm. (I) Graph showing average tubule cross-sectional area of P24 control versus cKO testes (n=20 tubules each from 3 independent males). (J) Graph showing cell counts of SOX9+ cells per tubule in P24 control versus cKO testes (n=15 tubules each from 3 independent males). (K) Graph showing percent of tubules displaying SOX9+ Sertoli cells mislocalizing to the tubule lumen in P24 control versus cKO testes (n=20 tubules each from 3 independent control males and n=50 tubules each from 3 independent cKO males). (L) Graph showing average number of GFRA1+ germ cells per tubule (in tubules that contained GFRA1+ cells) in P24 control versus cKO testes (n=25 tubules each from 3 independent males). (M) Graph showing percent tubules containing cleaved Caspase 3+ cells and cleaved Caspase 3+/TRA98+ double-positive germ cells in P24 control versus cKO testes (n=50 tubules each from 3 independent males). Data are shown as mean ± SD. *P* values were calculated using a two-tailed Student t-test.

Figure S6

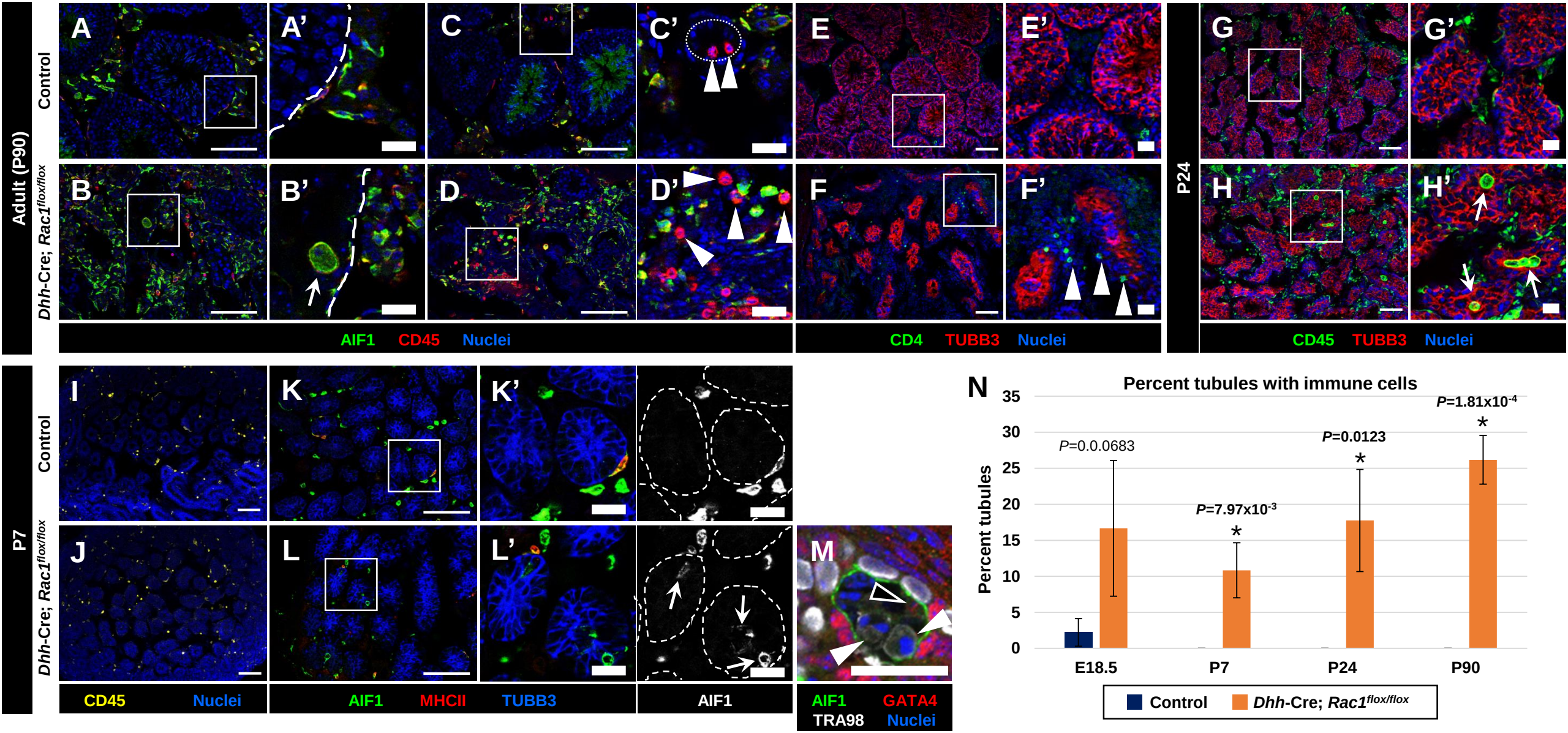
Adult (P90)
Control
Dhh-Cre; Rac1flox/flox
A
A'
C
C'
E
E'
B
B'
D
D'
F
F'
AIF1 CD45 Nuclei
CD4 TUBB3 Nuclei
P24
G
G'
H
H'
CD45 TUBB3 Nuclei
P7
Control
Dhh-Cre; Rac1flox/flox
I
K
K'
J
L
L'
M
CD45 Nuclei
AIF1 MHCII TUBB3
AIF1
AIF1 GATA4
TRA98 Nuclei
N
Percent tubules with immune cells
Percent tubules
35
30
25
20
15
10
5
0
P=0.0.0683
P=7.97x10-3
P=0.0123
P=1.81x10-4
*
E18.5
P7
P24
P90
Control
Dhh-Cre; Rac1flox/flox

Figure S6. Immune cells infiltrate into tubules of *Rac1* cKO testes, Related to Figure 6.

(A-M) Immunofluorescence images of P90 control *Dhh*-Cre;*Rac1*$^{flox/+}$ (A,C,E), P90 *Dhh*-Cre;*Rac1*$^{flox/flox}$ cKO (B,D,F), P24 control *Dhh*-Cre;*Rac1*$^{flox/+}$ (G), P24 *Dhh*-Cre;*Rac1*$^{flox/flox}$ cKO (H), P7 control *Rac1*$^{flox/flox}$ (I,K), and P7 *Dhh*-Cre;*Rac1*$^{flox/flox}$ cKO (J,L,M) testes. A'-H' and K'-L' are higher-magnification images of the boxed regions in A-H and K-L. (A-D) There is an increase in CD45+/AIF1+ macrophages in the adult cKO testis, in particular within the tubule lumen (arrow in B'), which are not observed in controls. (C,D) Round CD45-bright cells are more often seen in the interstitium of adult cKO testes (arrowheads in C' and D'), whereas they are only seen within arterioles in control testes (dashed outline in C'). (E,F) CD4 staining reveals an increase in T cell infiltration in cKO testes (arrowheads in F'). (G,H) P24 cKO testes contain an increased number of CD45+ cells, especially within tubule lumens (arrows in H'). (I-M) At P7, there appears to be a similar overall number of CD45+ cells (I,J) and AIF1+/MHCII+ macrophages (K,L) in controls versus cKO testes. However, there are macrophages within the tubule lumen (dashed outlines in K' and L') only in cKO testes (arrows in L'), which engulf both Sertoli cells (black arrowhead in M) and TRA98+ germ cells (white arrowheads in M). Thin scale bar, 100 μm; thick scale bar 25 μm. (N) Graph showing average percent of tubules containing immune cells in control versus cKO tubules at E18.5, P7, P24, and P90 (E18.5: n=40 tubules each from 3 independent males; P7: n=40 tubules each from 3 independent males; P24: n=40, 36, 39 tubules each from 3 independent males; P90: n=27, 36, 37 tubules each from 3 independent males). Data are shown as mean ± SD. *P* values were calculated using a two-tailed Student t-test.

Figure S7

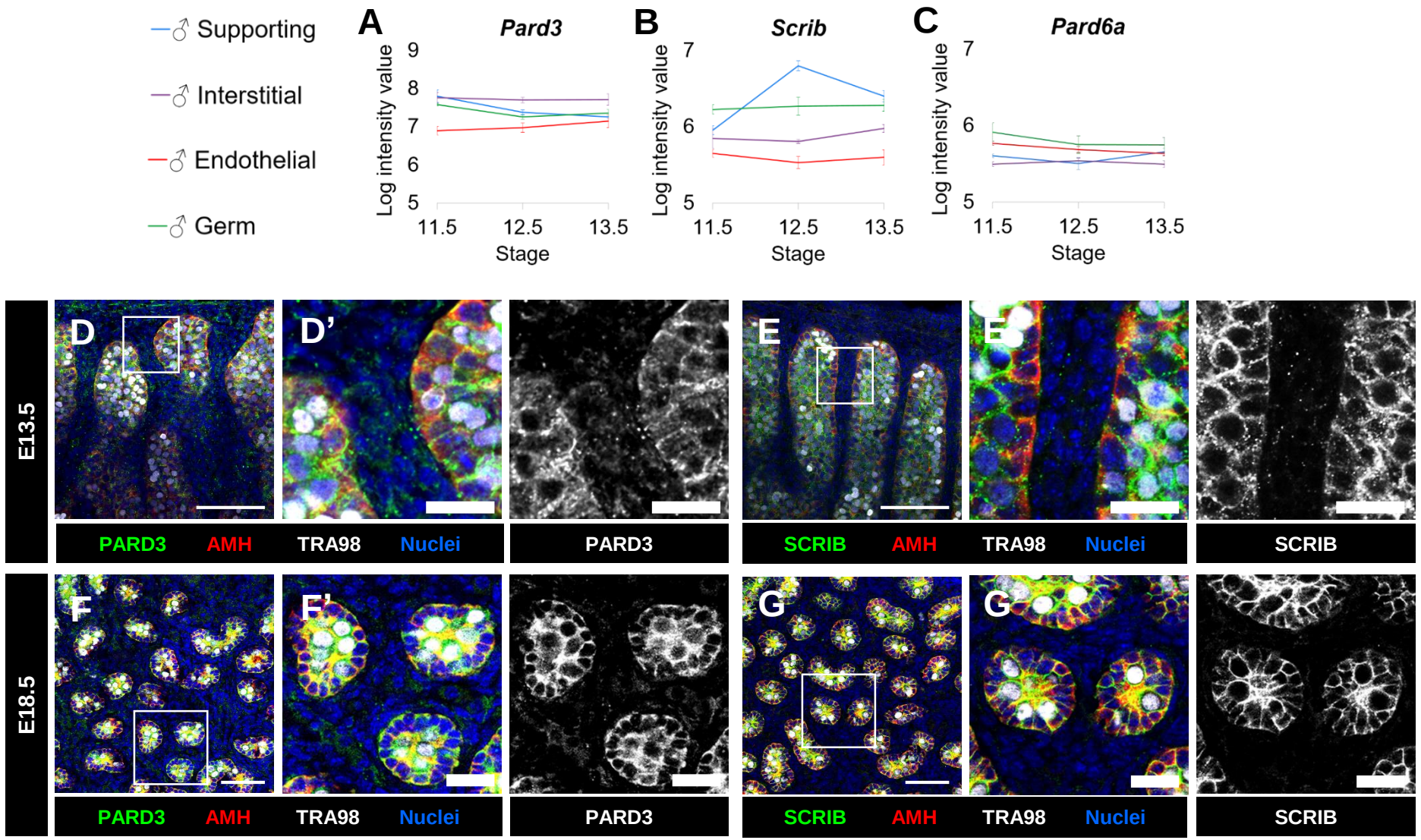
Supporting
Interstitial
Endothelial
Germ
A
Pard3
B
Scrib
C
Pard6a
Log intensity value
Stage
11.5
12.5
13.5
E13.5
E18.5
D
D'
E
E'
F
F'
G
G'
PARD3
AMH
TRA98
Nuclei
SCRIB

Figure S7. Apicobasal polarity markers are not specifically localized in fetal Sertoli cells, Related to Figure 7.

(A-C) Plots showing expression levels of apicobasal cell polarity genes *Pard3* (*Par3*), *Scrib* (*Scribble*), and *Par6da* (*Par6*), which were generated from fetal gonad cell-type-specific microarray data (Jameson et al., 2012), where cell lineages (supporting Sertoli cells, interstitial cells, endothelial cells, and germ cells) were independently plotted in different colors. Graph contains data for E11.5, E12.5, and E13.5 XY gonads for each cell type. In general, expression values below 6 are considered background expression levels. Overall, cell polarity genes in the fetal testis are either expressed non-specifically, i.e., in additional cell types other than Sertoli cells, and/or at very low/background levels. (D-G) Immunofluorescence images of E13.5 CD-1 (D,E) and E18.5 *Dhh*-Cre; $Rac1^{flox/+}$ control (F,G) fetal testes. D'-G' are higher-magnification images of the boxed regions in D-G. Apicobasal polarity markers PARD3 (apical) and SCRIB (basal) are both expressed in Sertoli cells at E13.5 and E18.5, but do not exhibit any specific subcellular localization or apicobasal enrichment. Thin scale bar, 100 μm; thick scale bar 25 μm.

Gene name	Sequence (5' to 3')
Amh forward	CCACACCTCTCTCCACTGGTA
Amh reverse	GGCACAAAGGTTCAGGGGG
Ar forward	CAGGAGGTAATCTCCGAAGGC
Ar reverse	ACAGACACTGCTTTACACAACTC
Cdh5 forward	TCCTCTGCATCCTCACTATCACA
Cdh5 reverse	GTAAGTGACCAACTGCTCGTGAAT
Cyp11a1 forward	GGAGGAAGCCGACAACAATGA
Cyp11a1 reverse	TCCACCTCACACGGTTCTCAA
Cyp17a1 forward	CAGAGAAGTGCTCGTGAAGAAG
Cyp17a1 reverse	AGGAGCTACTACTATCCGCAAA
Ddx4 forward	TACTGTCAGACGCTCAACAGGA
Ddx4 reverse	ATTCAACGTGTGCTTGCCCT
Dhh forward	GGCGCAGACCGCCTGATG
Dhh reverse	AAGGCACGGCCTTCGTAGTGG
Fshr forward	GGGATCTGGATGTCATCACT
Fshr reverse	GGAGAACACATCTGCCTCTA
Gapdh forward	AGGTCGGTGTGAACGGATTTG
Gapdh reverse	TGTAGACCATGTAGTTGAGGTCA
Gata1 forward	TGGGGACCTCAGAACCCTTG
Gata1 reverse	GGCTGCATTTGGGGAAGTG
Gdnf forward	GACTTGGGTTTGGGCTATGA
Gdnf reverse	AACATGCCTGGCCTACTTTG
Gfra1 forward (P7 assays)	CACTCCTGGATTTGCTGATGT
Gfra1 reverse (P7 assays)	AGTGTGCGGTACTTGGTGC
Gfra1 forward (P90 assays)	CCAATGTATCGGGCAGTACACA
Gfra1 reverse (P90 assays)	CCAGCGAGACCATCCTTTCC
Id4 forward	CAGTGCGATATGAACGACTGC
Id4 reverse	GACTTTCTTGTTGGGCGGGAT
Inhbb forward	GAGCGCGTCTCCGAGATCATCA
Inhbb reverse	CGTACCTTCCTCCTGCTGCCCTT
Kit forward	CATGGCGTTCCTCGCCT
Kit reverse	GCCCGAAATCGCAAATCTTT
Pdgfa forward	GACGGTCATTTACGAGATACCTC
Pdgfa reverse	CTACGCCTTCCTGTCTCCTC
Pou5f1 forward	GGAGGAAGCCGACAACAATGA
Pou5f1 reverse	TCCACCTCACACGGTTCTCAA
Sox9 forward	GCGGAGCTCAGCAAGACTCTG
Sox9 reverse	ATCGGGGTGGTCTTTCTTGTG
Srd5a1 forward	GAGTTGGATGAGTTGCGCCTA
Srd5a1 reverse	GGACCACTGCGAGGAGTAG
Stra8 forward	GCAGGTTGAAGGATGCTTTGAGC
Stra8 reverse	CCTAAGGAAGGCAGTTTACTCCCAGTC

Table S1. qPCR primers used in this study, Related to STAR Methods. Sequences of primers used for quantitative real-time PCR (qPCR) in this study (in alphabetical order).